

Phenophase-based comparison of field observations with satellite-based actual evaporation estimates of a natural forest: Miombo forest, southern Africa

Henry Zimba^{1,2}, Miriam Coenders-Gerrits¹, Kawawa Banda³, Bart Schilperoort¹, Nick van de Giesen¹, Imasiku Nyambe³, Hubert. H. G. Savenije¹.

¹ Delft University of Technology, Water Resources Section, Building 23 (Faculty of Civil Engineering and Geosciences) 2628 CN Delft, P.O Box 5048 2600 GA Delft, The Netherlands.

² Ministry of Agriculture, Department of Agriculture, P.O Box 50595, Mulungushi House, Independence Avenue, Lusaka, Zambia.

³ University of Zambia, Integrated Water Resources Management Centre, Department of Geology, School of Mines, Great East Road Campus, Lusaka, Zambia.

*Corresponding author: h.m.zimba@tudelft.nl

The trend and magnitude of actual evaporation across the phenophases of the Miombo forest are unknown. This is because estimating forest evaporation in African ecosystems continues to be a challenge as flux observation towers are scant, if not completely lacking in most ecosystems such as the Miombo forest. Furthermore, significant phenophases-based discrepancies in both trend and magnitude exist among the satellite-based evaporation estimates (i.e., GLEAM, MOD16, SSEBop and WaPOR) making it difficult to ascertain which of the estimates are close to field conditions of the Miombo forest. Despite the many limitations with estimation of forest evaporation the development and application of the distributed temperature system (DTS) is providing deepened insights and improved accuracy in forest energy partitioning for evaporation assessment. In this study the Bowen ratio distributed temperature sensing (BR-DTS) approach is used to partition available energy and estimate actual evaporation across three forest canopy phenophases of the Miombo forest covering the entire 2021 dry season (May – October) and early rain season (November – December). Furthermore, four satellite-based evaporation estimates are compared to the field observations. Our results show that that actual evaporation in the Miombo forest appears to follow the trend of the net radiation with the lowest values observed during the phenophase with lowest net radiation and the highest values during the phenophase with peak net radiation. It appears the continued transpiration during the driest period in the dormant phenophase (with lowest forest canopy cover and photosynthetic activities) may be influenced by the species dependent adapted physiological attributes such as access to moisture in deep soils (i.e., deep rooting), vegetative water storage and the variations in leaf fall and leaf flush. Of the four satellite-based evaporation estimates only the WaPOR has a similar trend to field observations across the three phenophase. However, all four satellite-based estimates underestimate the actual evaporation during the dormant and green-up phenophases. Large coefficients of variation among the satellite-based estimates appear to be in the dormant and green-up phenophases and are indicative of the difficulty to estimate actual evaporation in these phenophases. The differences between field observations and satellite-based evaporation estimates can be attributed to the model structure, processes and inputs.

1 Introduction

Global terrestrial evaporation is about 60 percent of the total incoming precipitation (Miralles *et al.*, 2011; Van Der Ent *et al.*, 2014). Evaporation in Africa, Asia and South America accounts for 78 percent of this terrestrial evaporation (Miralles *et al.*, 2011). A general paucity of

evaporation flux observation towers exists across the vast spectrum of ecosystems. As a consequence, several satellite-based evaporation estimates (e.g., GLEAM, MODIS, SEBop), in most cases, are used in hydrological modelling and water resources management without validation with field observations from the African ecosystems. In the face of climate change, accurate information on evaporation dynamics in major ecosystems, like the Miombo forest in southern Africa, with significant influence on basin hydrology, is important in the management of scarce water resources. Some studies have been conducted to validate satellite-based evaporation estimates in Africa (e.g., Blatchford *et al.*, 2020; Dile *et al.*, 2020; Weerasinghe *et al.*, 2020; Ramoelo *et al.*, 2014). However, none of these studies used field observations based on the Miombo forest evaporation. In southern Africa, the Miombo forest is the largest dry forest formation (Frost, 1996) and the characteristic vegetation cover for many river basins, including the Zambezi Basin. Miombo ecosystem with its unique plant-water interactions, differs from other ecosystems in Africa (Tian *et al.*, 2018; Vinya *et al.*, 2018). This means that the Miombo forest gives evaporation feedback incomparable to other ecosystems. The typical characteristics of the Miombo species leaf phenology are that they shed off leaves (leaf fall), grow new leaves (leaf flush) and also changes colour during what is normally termed the transition period in the dry season (May – October). The leaf fall and leaf flush are species dependent, occurring at different times in the dry season. Therefore, the variations in times for leaf fall and leaf flush means that the forest stand has about 70 percent canopy cover at any given period of the year. Depending on rainfall received in the preceding rain season, the leaf fall and leaf flush processes may start early (i.e., in case of low rainfall received) or late (in case of high rainfall received) and may extend into November (i.e., in the case of high rainfall received) (Frost, 1996; White, 1983). The evaporation dynamics in these phenophases have not been studied, but given the need for assessing the limited water resources in the ecosystem, there is a clear need for a detailed understanding of the phenophase-based evaporation in the Miombo forest. Yet, estimating evaporation over natural vegetation such as the Miombo forest in Southern Africa remains a challenge.

Limitations can be found in all available conventional approaches, such as the eddy covariance (EC) system (Foken, Aubinet, and Leuning, 2012), lysimeters (Sutanto, Wenninger, and Uhlenbrook, 2012; Teuling, 2018) and the conventional Bowen ratio (Bowen, 1926). For instance, inability to account for energy fluxes near the observation tower causes energy closure problems in the EC-systems. Furthermore, if the optical path is obscured, such as occurs in wet conditions, the EC's optical open-path sensors do not work properly and if the open-path analyzer is wet the evaporation which occurs shortly after a rainfall event is not observed (Coenders-Gerrits, Schilperoort, and Jiménez-Rodríguez, 2020; Hirschi *et al.*, 2017). In the case of the two vertical sensor-based Bowen ratio, each sensor has its own errors which are propagated to the Bowen ratio. Additionally, it is difficult to ensure that the two sensors are correctly aligned with each other which results in incorrect Bowen ratio estimates (Angus and Watts, 1984; Spittlehouse and Black, 1980). However, recent advances in the distributed temperature sensing system has expanded possibilities for improved accuracy in energy partitioning and the application of the Bowen ratio for evaporation flux assessment in forests (Euser *et al.*, 2014; Schilperoort *et al.*, 2020; Schilperoort *et al.*, 2018). In contrast to the conventional Bowen ratio approach, the Distributed Temperature Sensing Bowen ratio technique (BR-DTS) makes use of several vertical high resolution temperature measurements made with a single fibre optic cable. This eliminates the need for the conventional configuration with two individual sensors at different locations and the associated errors with this type of set up. One section of the fibre optic cable measures the air temperature profile, while a second section, covered in a constantly wetted cloth, measures the

wet-bulb temperature profile. The vapour pressure profile can be derived through the psychrometer principle. The DTS technique enables that wet and dry bulb temperature measurements can cover the entire vertical profile through a forest stand: above the forest canopy, within the canopy, and under the canopy. This is conducted simultaneously along a single fibre optic cable, thereby facilitating a deepened understanding of the energy partitioning in a forest (Schilperoort *et al.*, 2020; Schilperoort *et al.*, 2018; Euser *et al.*, 2014). Coenders-Gerrits *et al.* (2020) have suggested that the DTS technique offers opportunities to assess forest energy storage components that are not normally captured when using conventional approaches. The BR-DTS approach provides an avenue for enhanced understanding and increased accuracy in the estimation of forest evaporation. This is notwithstanding the challenges associated with the BR-DTS approach such as the requirement for sufficient ventilation and constant wetting of the fibre optic cable. Furthermore, compared to the EC method the BR-DTS approach tends to minimally overestimate diurnal latent heat flux (LE) by a mean difference of 18.7 Wm^{-2} (Schilperoort *et al.*, 2018).

For the Miombo forest, the need for field-based actual evapotranspiration estimates is augmented by the discrepancies in satellite-based evaporation estimates (Zimba *et al.*, 2022). Due to a lack of field-based observations of actual evaporation in the Miombo forest the satellite-based evaporation estimate(s) that are close to field conditions are unknown. Therefore, this study provided an independent estimation of Miombo forest actual evaporation that can be used to validate satellite-based evaporation estimates.

In this study field observations were compared to four commonly-used free satellite-based actual evaporation estimates: GLEAM (Martens *et al.*, 2017), MOD16 (Mu *et al.*, 2011), SSEBop (Savoca *et al.*, 2013) and WaPOR (FAO, 2018). The satellite-based estimates were selected because they can be obtained free of cost, have comparatively high spatial-temporal resolution, and good spatial coverage (i.e., global in the case of GLEAM, MODIS, SSEBop and continental in the case of WaPOR), and are ready-to-use products with no further processing required. Hence, the focus of our study was on characterising the Miombo forest actual evaporation using the BR-DTS approach, and comparing the field observations to the satellite-based evaporation estimates. Consequently, objectives of this study were to:

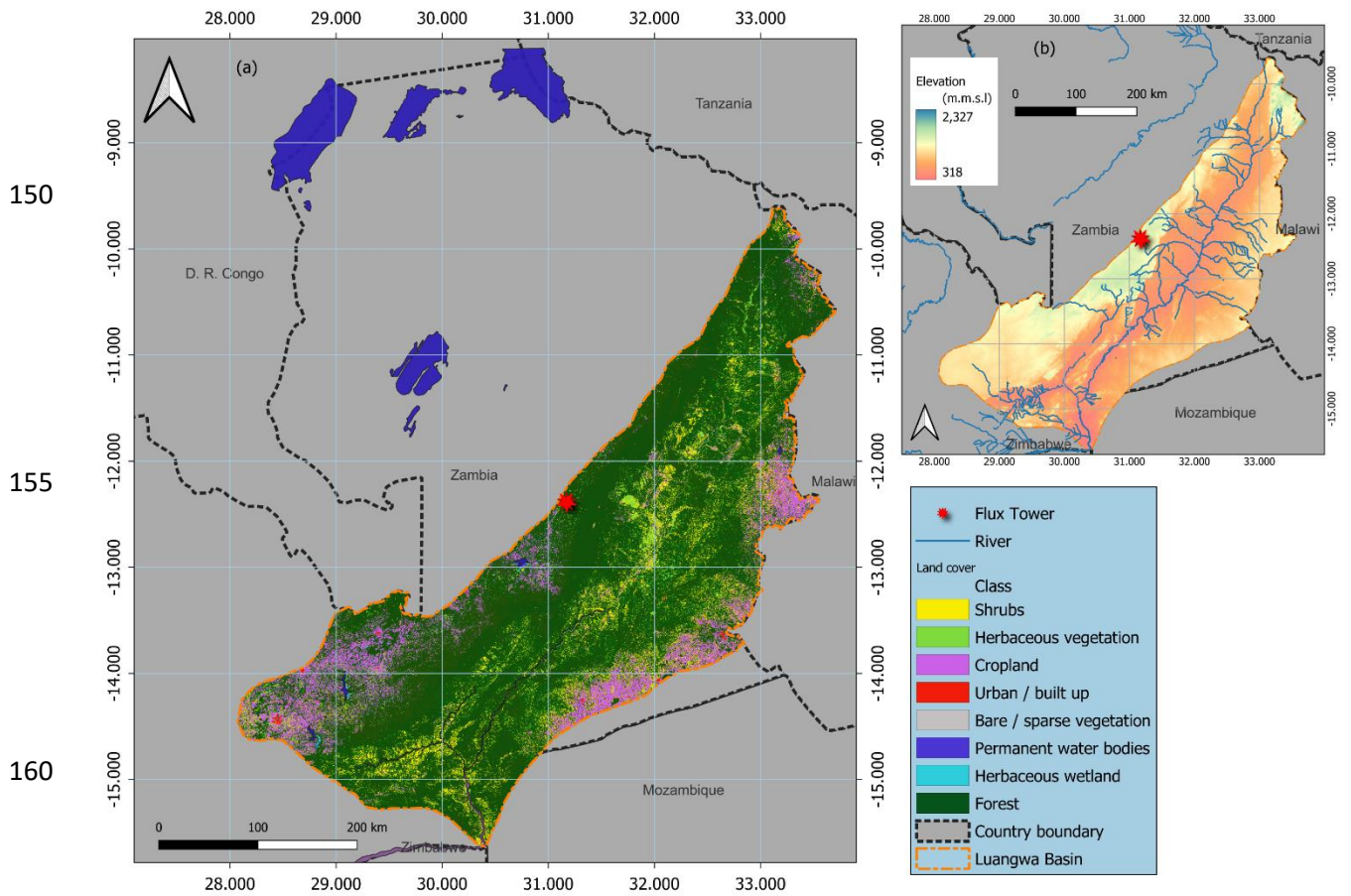
- (i) Estimate the actual evaporation of the Miombo forest across forest canopy/leaf phenophases to help understand the flux trend and magnitude in the ecosystem,
- (ii) Compare free satellite-based evaporation estimates to the field-based estimates at point scale across the canopy/leaf phenophases of the Miombo forest.

2 Materials and methods

2.1 Study site

The study was centred on a dense Miombo forest at the Nsanzala and Mutinondo conservancy areas (lat: -12.38° S , long: 31.17° E) in the Mpika District, northern Zambia in southern Africa (Fig. 1). Zambia was selected because it is considered to have the largest diversity in Miombo forest species composition (Frost, 1996; White, 1983). The site in Mpika was chosen because it represents a large area of undisturbed Miombo forest with high heterogeneity in species typical of Miombo forest. It is also situated in the largest Miombo ecosystem component of the wetter central Zambezian Miombo (Olson *et al.*, 2001; White, 1983), in the north-western part of the Luangwa Basin (Fig. 1). At the study site, species identification and counts within a 250m-by-250m sample plot showed that over 95 percent of the dominant Miombo species is semi-deciduous and include: *Brachystegia floribunda*, *Brachystegia longifolia*, *Brachystegia boehmii*,

140 *Brachystegia speciformis*, *Jubenerdia panincolata*, *Uapaca kirkiana*, *Pericopsis angolensis*,
Bauhinia petersenia and *Uapaca sansibarica*. These are typical Miombo species, especially the
Brachystegia floribunda, found in the wetter Zambezi Miombo Woodland (White, 1983). The
typical characteristics of the Miombo species at the site are that they shed off leaves (leaf fall) and
also leaf flush during what is termed as the transition period in the dry season (May – October).
145 Frost (1996) indicated that, based on the amounts of rainfall received in the preceding rain season,
the leaf-fall and leaf flush processes may start early (i.e., in case of low rainfall received) or late
(in case of high rainfall received) and may extend up to November (i.e., in the case of high rainfall
received).



165 **Figure 1.** Land cover (a) and elevation (b) characterisation in the Luangwa Basin and at the study
site in Mpika. The ASTER Digital elevation model was used to depict elevation while the 2019
Copernicus Land cover for Africa was used for land cover characterization.

170 Elevation ranges between 318 m and 2327 m above sea level (Fig. 1 b). The study site has a mean
annual rainfall of 1200 mm year⁻¹ and mean annual temperature of 26 °C. Rainfall is a result of the
movement of the intertropical convergence zone (ITCZ) over Zambia. Rainfall period is between
October and April while the dry season is between May and October (Hachigonta and Reason,
2006; Chidumayo, 2001). The forest at the study site is ~~characteristically~~ undisturbed by ~~extremely~~
~~limited~~ anthropogenic activities due to the site being a conservancy. The major activities in the
area are controlled cattle ranching and tourism. Controlled burns are normally conducted in August

175 when the Dambos (wetlands) are dry, and are mainly conducted in the Dambo grassland for
livestock grazing purposes.

2.2 Study approach

180 This study compared estimates of actual evaporation by the BR-DTS method with the
Penman-Monteith reference evaporation (Allen *et al.*, 1998) and to four satellite-based evaporation
estimates at point scale in the Miombo forest. The observations were conducted for the period May
to December 2021. The study period facilitated assessment of evaporation during the wet and dry
seasons across three different Miombo forest phenophases. The Collection 6 MODIS Land Cover
Dynamics (MCD12Q2) Product (Gray *et al.*, 2019), Zimba *et al.* (2020) and the field observations
of the Miombo forest canopy were used to characterise the phenophases. The phenophases in this
study were based on data gathered between May-December 2021 and were categorised into three
groups i.e., green-down (May-June), dormant (July-September) and green-up/mid-green-up
(October -December). For ease of comparison to satellite-based evaporation estimates the green-
up phenophase included the early maturity phenophase, which is generally attained around
190 December, when consistent rainfall is experienced.

2.3 Estimating potential evaporation

The Penman-Monteith (PM) equation (i.e., Eq. 6 in Allen *et al.*, 1998) was used to estimate
reference evaporation (E_o) from which potential evaporation for the Miombo forest was calculated
195 using Eq. (1). All required inputs for the PM equation were obtained at the study site. To obtain
potential evaporation for the Miombo forest the crop coefficient (K_c) value of 0.8 was used. The
 K_c value used was obtained from literature (Hunink *et al.*, 2015). The K_c was estimated based on
the Miombo forest in Mahele, Tanzania. The K_c for the Mahele region in Tanzania was utilised
because it situated in the wet Miombo region receiving rainfall of about 1000 mm year⁻¹, with
200 similar seasonality as the study site in Mpika in which rainfall starts late October and ends early
May (Hunink *et al.*, 2015). Furthermore, despite its vast expanse there is unexpectedly little
variation in Miombo forest species diversity (Chidumayo and Gumbo, 2010). In this study the
same K_c value was applied for the dry and the rainy season.

$$205 \quad E_{c(PM)} = K_c \cdot E_o \quad (1)$$

2.4 Conventional Bowen ratio energy balance method

The Bowen ratio is the proportion of the sensible (H) to the latent heat flux (LE) of a
surface. In simple form the Bowen ratio can be determined by multiplying the psychrometric
210 constant by the ratio of the temperature and vapour pressure gradients as expressed in Eq. (2):

$$\beta \approx \gamma \cdot \Delta T_a / \Delta e_a \quad (2)$$

where γ is the psychrometric constant (kPaK⁻¹) (Eq. 3), ΔT_a is the difference in temperature (K)
between two heights and Δe_a is the difference in the actual vapor pressure (kPa) between the same
215 two heights. The psychrometric constant is obtained using the relationship between air pressure
and ventilation of the psychrometer as given by Allen *et al.* (1998) in Eq. (3):

$$\gamma = 0.0665 \times 10^3 \cdot P \quad (3)$$

where, P is the atmospheric air pressure (kPa).

220 Despite the simplicity of the approach, the energy balance Bowen ratio method needs to meet several conditions in its application for results to be reliable. For instance, the two levels at which the temperature and vapor pressure are measured must be within the boundary layer of the air flow, which has adjusted to that particular land surface. The measurement site therefore requires extensive fetch in the upwind direction for the airflow over the land surface, in this case the forest canopy. A fetch of at least 100 times the maximum height of measurement is typically suggested
225 for such measurements (Angus and Watts, 1984).

2.5 BR-DTS energy balance approach

The BR-DTS method measures air temperature gradients directly and the vapour pressure gradients are estimated via the wet bulb temperatures using Eq. (4):

$$e_{a(T_a)} = e_{s(T_w)} - \gamma(T_a - T_w) \quad (4)$$

230 where $e_{a(T_a)}$ is the actual vapour pressure, $e_{s(T_w)}$ is the saturated vapour pressure, γ is the psychrometric constant, T_a and T_w are the dry bulb and wet bulb temperature. Details on this calculation can be found in Schilperoort *et al.* (2018).

In contrast to the conventional Bowen Ratio Energy Balance, where only the temperature and vapour pressure at two heights are used, the BR-DTS method uses all measuring points
235 between two heights. All dry and wet bulb temperatures within this segment are used to determine the gradients according to a natural logarithmic of the height (Eqs. 5 and 6):

$$T_{a_{fit}} = a \cdot \ln(z) + b \quad (5)$$

$$e_{a_{fit}} = c \cdot \ln(z) + d \quad (6)$$

240 The fitted DTS temperature and actual vapour pressure at 11 m (bottom) and 15.5 m (top) heights above the forest canopy were used to estimate the Bowen ratio following Eqs. (7) – (9):

$$\beta = \gamma \cdot \frac{\Delta T_{a_{fit}} / \Delta z}{\Delta e_{a_{fit}} / \Delta z} \quad (7)$$

in which;

$$\Delta T_{a_{fit}} / \Delta z = T_{a_{fit}}(z=\text{top}) - T_{a_{fit}}(z=\text{bottom}) / (z=\text{top} - z=\text{bottom}) + \Gamma(z) \quad (8)$$

and

$$245 \frac{\Delta e_{a_{fit}}}{\Delta z} = \frac{e_{a_{fit}}(z=\text{top}) - e_{a_{fit}}(z=\text{bottom})}{z=\text{top} - z=\text{bottom}} \quad (9)$$

where $\Delta T_{a_{fit}}$ is the difference in air temperature (K) of the fitted curve between the bottom and top of the height range used for the Bowen ratio, $\Delta e_{a_{fit}}$ is the difference in actual vapor pressure (kPa) of the fitted curve over the same height as in temperature, Δz is the difference in height (m)
250 between the two points and Γ is the adiabatic lapse rate (normally around 0.01 Km^{-1}). During dry and unsaturated conditions, very small temperature and vapor pressure gradients could result in errors in the Bowen ratio estimates. The use of the lapse rate is recommended in such circumstances (Schilperoort *et al.*, 2018; Barr *et al.*, 1994). In this study the lapse rate was applied

255 throughout the study period following Schilperoort *et al.* (2018). Before fitting the raw DTS data
was calibrated following the approach by des Tombe *et al.* (2020).

2.6 DTS data quality control

260 The quality control process followed the demonstration by Schilperoort *et al.* (2018) as
shown in Eqs. (10) and (11). Only diurnal temperature and actual vapour pressure data (i.e.,
between 06AM and 18PM were considered). This is because night time actual evaporation was
not estimated, as it was assumed to be negligible. The correlation coefficient of determination (r^2)
values for fitted vapour pressure were used for quality control. The fitted actual vapour pressure
with r^2 values below 0.2 and Bowen ratio values approaching -1.1 and -0.9 were removed from
the data and gaps filled by the regression method. The coefficients (r^2) for dry and wet bulb
temperature were not considered because the high uncertainty in temperature is propagated in
265 vapour pressure.

$$\text{Flag 1: } r^2_{ea,z} > 0.20, \quad (10)$$

$$\text{Flag 2: } \beta < -1.1 \text{ or } \beta > -0.9. \quad (11)$$

2.7 Actual evaporation estimation

270 Several studies (i.e., Buttar *et al.*, 2018; Euser *et al.*, 2014; Xing *et al.*, 2008; Spittlehouse
and Black, 1980) demonstrated the use of the Bowen ratio in combination with the energy balance
to assess the latent heat flux. In combination with other energy terms the Bowen ratio energy
balance estimate of evaporation (E_β) can be conducted using Eq. (12):

$$E_\beta = (R_n - M - G_s)/L(1 + \beta) \quad (12)$$

275 where R_n is the net radiation flux (Wm^{-2}), L being the latent heat of vaporization of water (2.45
 MJkg^{-1}), G_s is the ground heat flux (Wm^{-2}) and the M is the change in energy storage in the system
canopy storage (Wm^{-2}). The ground heat flux in this study was estimated from the net radiation at
hourly intervals. For the Penman-Monteith model (Allen *et al.*, 1998), the ground heat flux for
hourly (G_{hr}) or shorter periods for reference/growing crop, can be estimated from net radiation
280 (R_n) using Eq. (13) during daylight and Eq. (14) during night-time periods. However, the G_s for
forests is different from that of grass or growing crop. Some studies, in different forests, found G_s
to be between 5 – 24 percent of R_n (i.e., Ma *et al.*, 2017; Van Der Meulen and Klaassen, 1996;
McCaughey, 1982). With reference to observed G_s in different forests, this study selected 10
percent of R_n for hourly daytime G_s . The 10 percent was selected because the Miombo forest at
285 the study site, at any period of the year, has about 70 percent canopy cover (Fuller, 1999; Frost,
1996). Furthermore, during the dry season (May-October), when there is reduction in canopy
cover, top soil (0 - 30 cm) moisture, was not expected to vary significantly.

$$G_{hr} = 0.1R_n \quad (13)$$

$$G_{hr} = 0.5R_n \quad (14)$$

290 we follow Schilperoort *et al.* (2018) in their observation that the change in change in canopy
storage (M) can be ignored. The E_β was estimated at hourly intervals and then summed up into
daily and 10-day values.

2.8 Comparison of satellite-based evaporation estimates

For comparison to satellite-based evaporation estimates, field actual evaporation estimates

295 were categorised into 10-day and monthly data sets to be in tandem with the satellite evaporation
 products temporal scales. The native spatial resolutions (Table 1) of the satellite-based evaporation
 estimates were used because these products are mostly applied or used in their native resolution
 configuration. All satellite-based estimates used in this study can be obtained free of cost and are
 readily available. In Africa, financial constraints are a resource limitation. Therefore, to have
 300 access to free of cost satellite evaporation products has significant advantage. Furthermore, in the
 context of this study, sufficient historical data was available and all products are continuously
 being processed which assures, to a large extent, future availability of data for continued
 monitoring. Except for the WaPOR, which had a continental spatial extent, the rest of the satellite-
 based evaporation estimates had global spatial extent. However, all four products adequately
 305 covered the extent of the Miombo forest, which was the focus of this study. All four satellite-based
 estimates were accessed online from different platforms as indicated in Table 1. Details of the
 methods for each satellite-based evaporation estimate can be found in the specific documents cited
 in Table 1.

2.9 Statistical analysis

310 The field observations and satellite-based evaporation estimates were compared using the
 Kendall and Pearson correlation coefficients, correlation coefficients of determination (R^2) (Eq.
 15), Root Mean Square Error (RMSE) (Eq. 16) and the mean bias error (MBE) (Eq. 17). These are
 some of the commonly used techniques for comparing pairs of variables and assessing
 performance of hydrological models (Helsel *et al.*, 2020). The coefficient of determination
 315 measures the strength of relationship between the observed with the modelled values. The
 relationship between variables is strongest as the R^2 value approaches 1. The RMSE quantifies the
 deviation of the predicted values from the observed values. The model predictions are more
 accurate as the RMSE value approaches zero. The mean bias error is the measure of the extent to
 which modelled values deviate from observed values and indicates whether there is under or
 320 overestimation. The smaller the mean bias error value the less the deviation of the predicted values
 from the observed values (Helsel *et al.*, 2020). Negative value indicates underestimation while a
 positive value indicates overestimation.

$$R^2 = 1 - \frac{\sum_i (O_i - P_i)^2}{\sum_i (O_i - \bar{O})^2} \quad (15)$$

325

$$RMSE = \sqrt{\frac{1}{n} \sum_{i=1}^n (p_i - o_i)^2} \quad (16)$$

$$MBE = \frac{1}{n} \sum_{i=1}^n (p_i - o_i) \quad (17)$$

330

where, O_i is the flux tower observed evaporation, \bar{O} is the mean of the observed evaporation, P_i is
 the modelled evaporation and n is the number of observations.

Table 1 Characteristics of satellite evaporation products used in this study

Evaporation product	Spatial coverage	Temporal resolution	Spatial resolution	Estimation approach	Source of input data	Reference	Source of data
SSEBop	Global	Decadal	1000 m	P-M equation, ET fractions from T_s estimates	MODIS	(Savoca et al., 2013).	Climate engine
Access: https://clim-engine.apps.spot.com/ClimateEngine (Accessed 2020)							
WaPOR v2.	Continental	Decadal	250 m	P-M Equation, calculates E, T and I separately	MODIS		WaPOR Portal
Access: https://wapor.apps.fao.org/home/WAPOR_2/1?theme=L1_AFTI_D&dim=DEKAD:%255B2020-08-11%252C2020-08-21							
GLEAM (v3.6a and v3.6b)	Global	Daily	27000 m	P-T equation, soil stress factor	AMSR-E, LPRM, MSWEP+MSWX	(Martens et al., 2017); (Miralles et al., 2011)	FTP server
Access: https://www.gleam.eu/							
MOD16	Global	8-day	500 m	P-M equation, surface conductance model	MODIS	(Mu et al., 2011)	Global subsets tool: MODIS/VIRS Land Products
Access: https://modis.ornl.gov/globalsubset/							

335

340

345

350

355

360

365

370

375 **2.10 Flux observation tower setup**

Temperature was measured using a single 3 mm 1 km long white jacket duplex single tube fibre optic cable connected to the DTS machine. The cable's ends were spliced together to loop the signal back making a double ended configuration. Double ended configuration was explained in (van de Giesen *et al.*, 2012). The DTS machine used is the Silixa XT-DTS (Silixa Ltd, 2016) with sensing capabilities as shown in Table A1 in the appendices. A calibration bath was set up in which 10 m of the fibre cable from the DTS was placed in water together with 2 x 2 PT-100 probes for the entire period of the measurements. The DTS was set to take temperature measurements at a 5 minutes interval. The fibre optic cable was firmly secured on a 17.25 m vertical tower (illustrated in Figs. 2 and 3) following the techniques demonstrated by Euser *et al.* (2014) and Schilperoord *et al.* (2018). One section of the fibre cable (blue line in Fig. 2) from the DTS machine was wrapped in cotton cloth (Fig. 3 a) starting at the base up to the top of the tower and was always kept wet for estimation of what is known as wet bulb temperature.

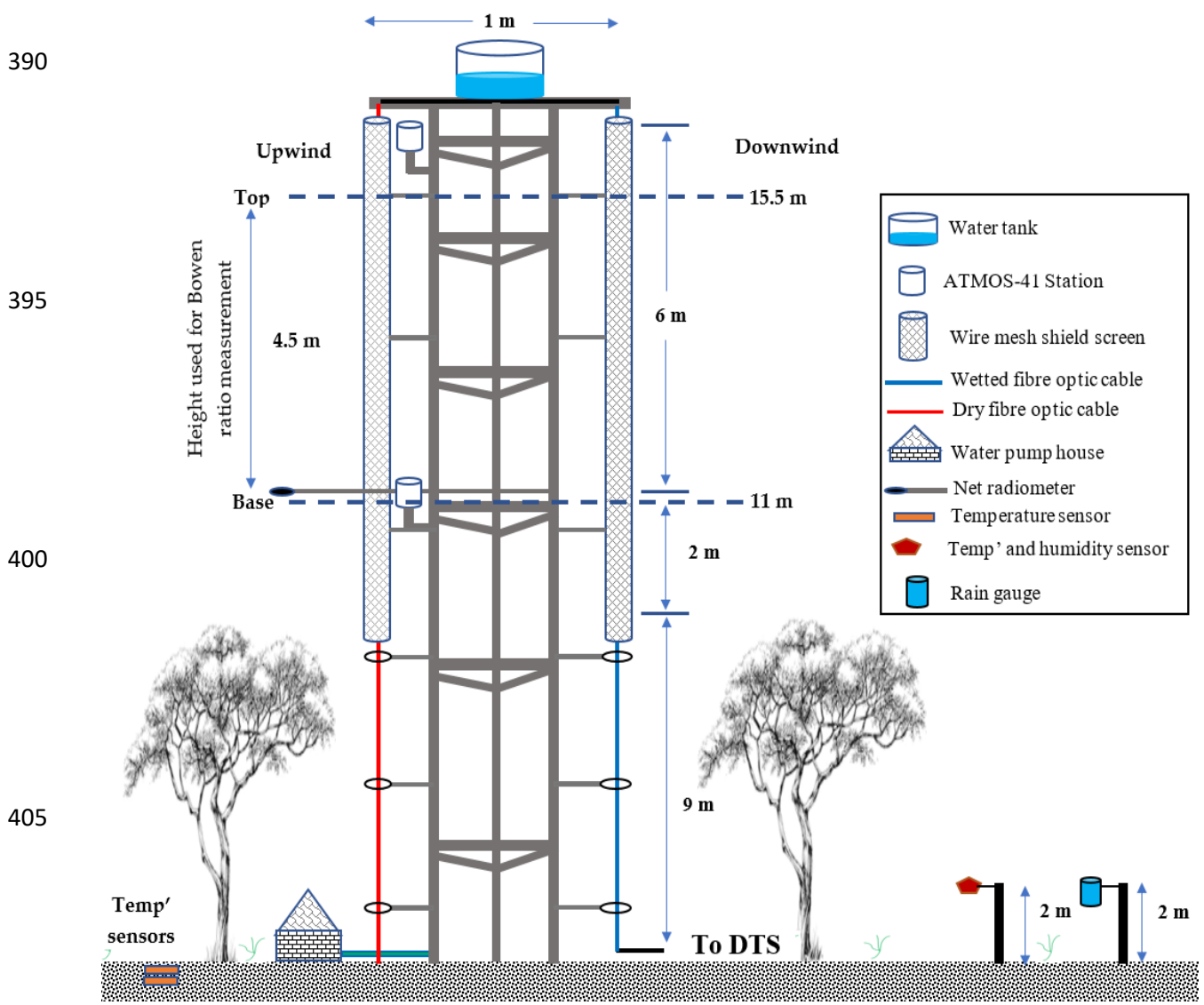


Figure 2. Schematic drawing (not to scale) of the field set-up of the observation tower at the study site in Mpika, Zambia.



Figure 3. Optic fibre cable wrapped in the wet cloth (a) for collecting the wet bulb temperature and (b) optic fibre cable not wrapped in cloth for estimating the dry bulb temperature on the observation tower at Mpika site, Zambia. Under canopy view without screens.

415

420

425

430

435

440

445

450

Separated by a 1 m gap the other section of the fibre cable (red cable in Fig. 2) was not wrapped (Fig.3 b) in a cotton cloth and was designated to measure the air temperature. The cloth on the designated wet cable was kept constantly wet by the water that was pumped to the 65-litre tank placed at the top of the tower. The water flow from the water tank to the fibre cable was regulated (roughly 20 litres per day) to ensure a smooth and constant wetting of the cotton cloth. As recommended by Euser *et al.* (2014) the wet cable was placed on the downwind side while the dry cable was placed on the upwind side of the tower. The type of cables arrangement prevented water from the wetted cotton cloth for the wet cable to splash onto the dry cable. This set up of cables ensured that the dry bulb temperature measurements were not affected. Furthermore, a gap of 1 m also contributed to ensuring that the dry cable was not affected by the water from the wetted cotton cloth. Following the recommendation by Schilperoort *et al.* (2018) both the wet and dry cable were shielded from direct sunlight by 8-meter long two layered wire mesh screens placed above the canopy (Fig. 2).

A portion of data, within 2 m of the top of the tower, was not included in the assessment because it was assumed to influence the wet clothe/wet cable temperature as the water from the tank above the tower was at a temperature slightly higher than the air temperature. The 2 m length was considered a sufficient length for the temperature of the water from the tank to be uniform with the environment and suitable for measurement of wet bulb temperature. For this study the tower height was 17.25 m and the fetch was beyond 1.7 km. The fetch was in an area with more than 20 km of uninterrupted Miombo Woodland with typical sporadic small seasonal wet grasslands (Fig. A1 b in the appendices). Furthermore, Spittlehouse and Black (1980) showed that greater accuracy in the Bowen ratio measurements could be attained by increasing the separation between, and interchanging the psychrometers. In this study it was ensured that more than 4 metres separation were between the two levels at which the temperature and actual vapour pressure were selected above the forest canopy.

To obtain the net radiation (R_n , Wm^{-2}) the NR Lite 2 net radiometer (Kipp & Zonen CNR4) was installed at about 2 m above the forest canopy (that is 11 meters from the forest floor) (Fig. 2). The net radiation was logged at an hourly interval using the Campbell CR10X data logger. With reference to estimates in other forests (i.e., Ma *et al.*, 2017; Van Der Meulen and Klaassen, 1996; McCaughey, 1982) an hourly ground heat flux (G_o , Wm^{-2}) was estimated at 10 percent of the hourly net radiation. The soil moisture was obtained using two HOBOnet ECH2O™ EC-5 soil moisture sensors placed at 5 cm and 30 cm in the soil sub-surface. The Onset HOBO S-THB-M002 smart sensors were used to measure under-canopy air temperature and relative humidity at 2 m above the ground and logged at a 5-minutes interval. Using the Onset HOBO S-RGA-M002 –rain gauge rainfall was measured at the flux tower site 2 m above ground and away from tree canopies (Fig. 2). The rain gauge was logged at a 5-minutes interval.

The air temperature and actual vapour pressure to compare with the DTS measurements were obtained using the METER Group AG ATMOS-41 all-in-one weather station sensors. The ATMOS-41 sensors meet standards for the World Meteorological organization (WMO). The accuracy of the ATMOS-41 is ± 0.6 °C for air temperature at below 40 °C and $\pm 3\%$ for relative humidity. Details on the capabilities of the ATMOS-41 sensors can be found in the manual (Meter Group AG, 2020). Characteristics of selected ATMOS-41 sensors are given in Table A2 in the appendices. Two ATMOS 41 stations were used, placed at 2 m above the forest canopy (11 meters from the forest floor) and at 8 meters above the canopy (16.5 meters from the forest floor) (Fig. 2). The ATMOS-41 station sensors were logged at a 5-minutes interval same as the DTS.

3 Results and discussion

3.1 Evaporation flux foot print/Fetch analysis

500 An analysis of the evaporation flux foot print was performed using the wind rose (Fig. A1 in the appendices). The wind rose was used to obtain the most frequent and consistent wind direction to help determine which part of the study site ~~was the major influencer of~~ the evaporation flux. The wind was predominantly coming from the eastern direction with wind speed ranging between 2 – 6 m s⁻¹. ~~This~~ made it possible to obtain satellite product values in the correct grids/pixels for comparison with BR-DTS evaporation estimates $E_{a(DTS)}$. Using the identified
505 predominant wind direction, the fetch/flux footprint equal to 100 times the height (17.25 m) of the observation tower was designed. Thus, the fetch/flux footprint was designed to cover a 1.725 by 1.725 km area (approximately 2 km by 2 km grid).

3.2 DTS data quality control

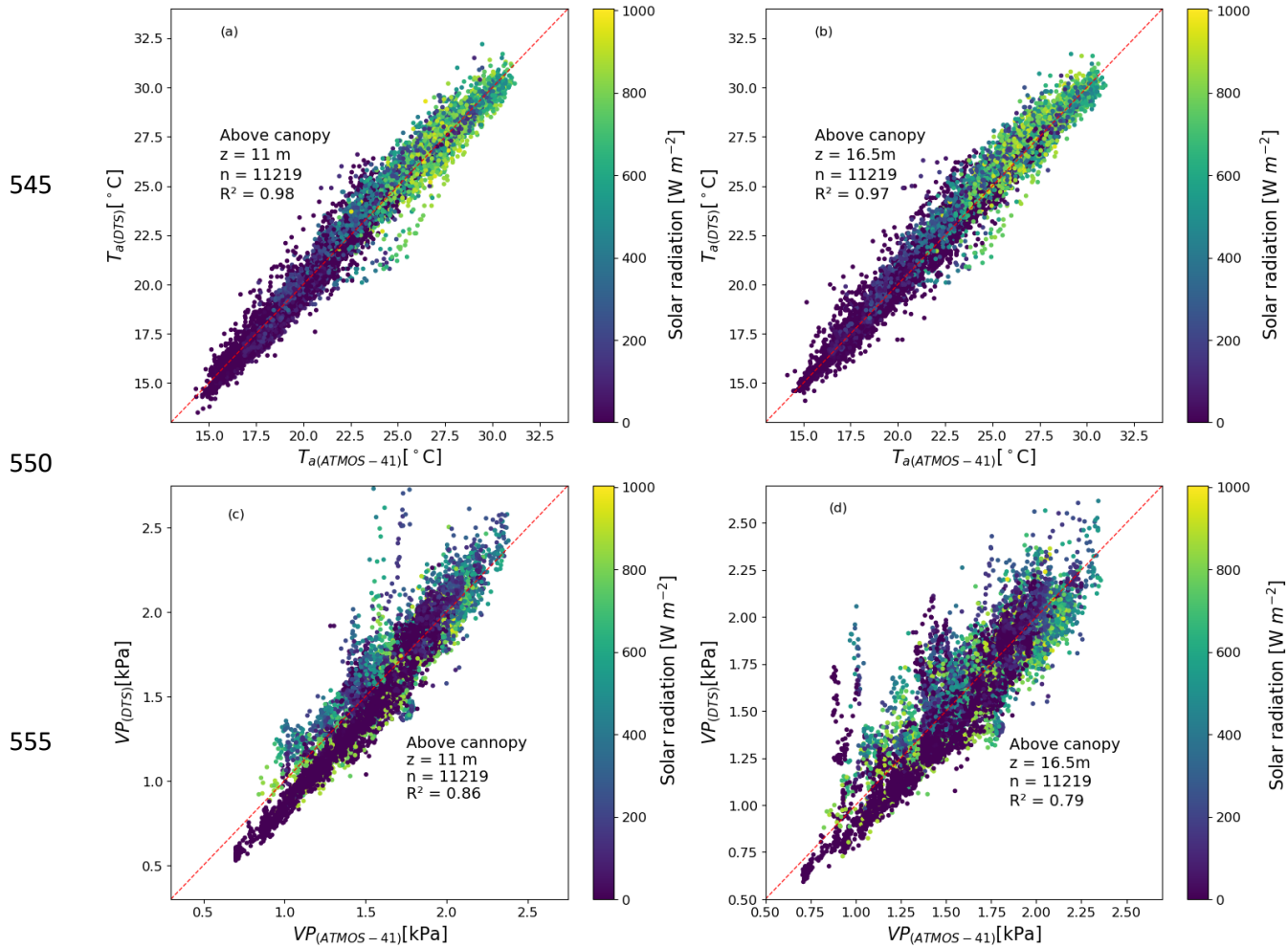
510 The DTS measurements were conducted from 1 May to 25 December, 2021. Following the quality control processes by Schilperoort *et al.* (2018), DTS data for seven days (2 in June, 2 in August, 2 in September and 1 in October) did not pass the quality test. These data were collected on the days when challenges of keeping the entire wet fibre cable cloth constantly wet were experienced. The data were removed and gaps filled by the linear regression method. Due to challenges with power supply for the DTS machine, six days in December (26th to 31st) were not
515 available for analysis.

3.3 Comparison of DTS-based estimates with the ATMOS-41 estimates

DTS estimates of air temperature and actual vapour pressure were compared with the ATMOS41 estimates at 11 m and 16.5 m heights above the forest canopy on the tower (Fig. 2). At height 16.5 m the DTS-based estimates and the ATMOS-41-based estimates showed relatively
520 lower correlation ($R^2 = 0.97$; 0.79 for air temperature and actual vapour pressure respectively). However, at 11 m the correlation coefficients ($R^2 = 0.98$; 0.86 for air temperature and actual vapour pressure respectively) were relatively higher (Fig. 4 a - d). The lower correlation coefficients at 16.5 m may be explained ~~the installing~~ ATMOS-41 weather stations above the forest canopy that exposed the temperature
525 sensors to direct sunlight in early morning and late afternoon. This influenced the temperature measurements and resulted in deviations in ATMOS-41 air temperature for the two periods. Additionally, the water from the tank on the tower did not always reach the wet bulb temperature at the 16.5 m height resulting the overestimation of the DTS-based actual vapour pressure. Overall, the DTS and ATMOS-41-based estimates, at both heights, showed good agreement, sufficient for this study. The accuracy properties of the ATMOS-41 are shown in Table
530 A2 in the appendices.

535

540



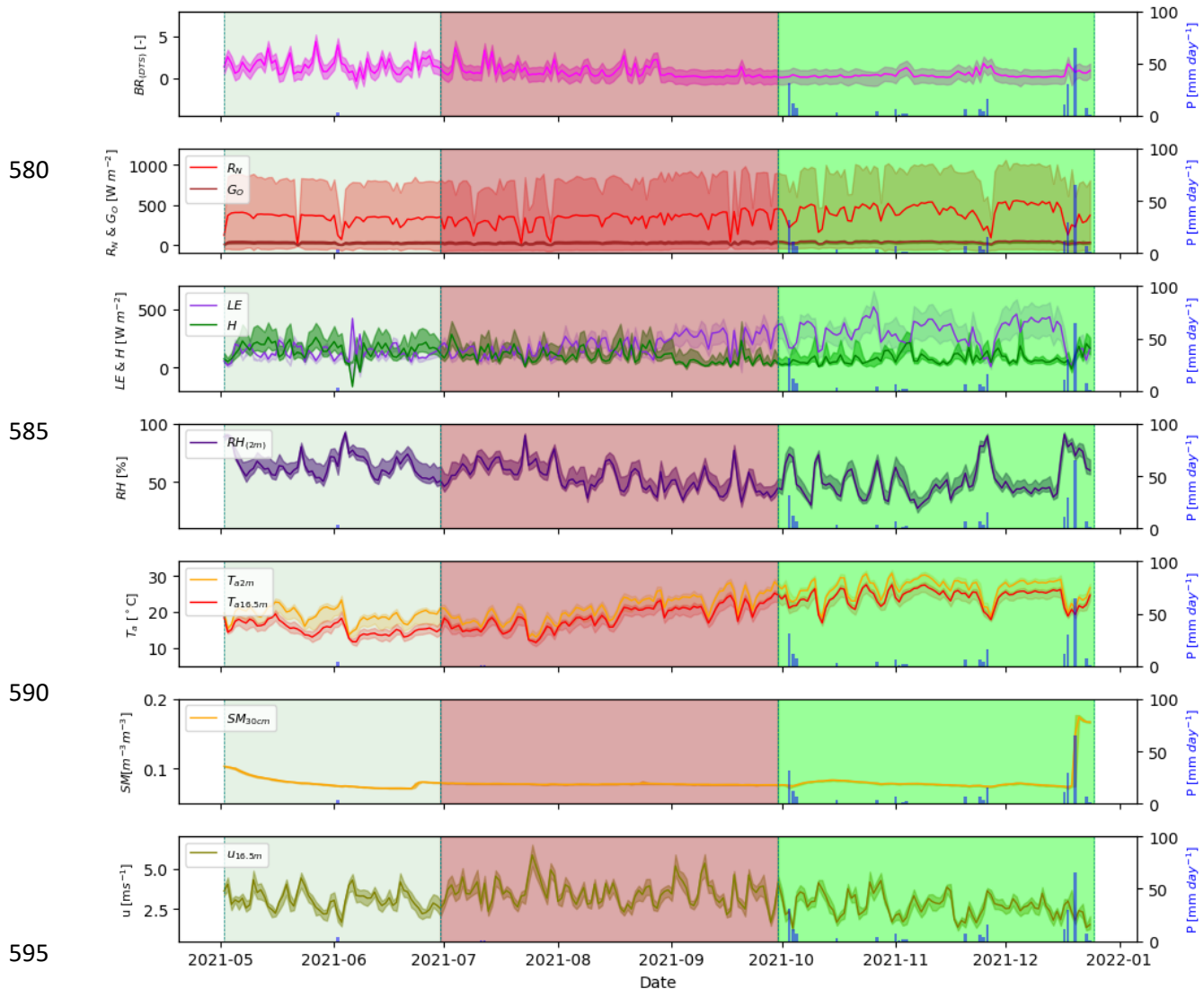
560 **Figure 4.** Comparison of DTS temperature ($T_{a(DTS)}$) and actual vapour ($VP_{(DTS)}$) measurements
 565 with the *ATMOs-41* ($T_{a(ATMOs-41)}$ and $VP_{(ATMOs-41)}$) measurements at 11 m and 16.5 m above
 the forest canopy.

3.4 Meteorological conditions

565 The wind direction was mainly between the North-East and South-East direction (approx.
 50 – 110 degrees) (Fig. A1 in the appendices). Wind speed (u) ranged between 0.7 - 8 m s⁻¹ with
 relatively higher speeds observed in the dry season between July and September during the
 dormant phenophase (Fig. 5). Minimum and maximum net radiation (R_N) were observed during
 the dry season and wet season respectively. The drop in air temperature (T_a) and relative humidity
 (RH) coincided with reduced soil moisture (SM) in the dormant phenophase in the dry season (Fig.
 570 5). T_a ranged between 7 – 32° C. Relative humidity negatively co-varied with T_a and R_N .

Using the DTS-based Bowen ratio (BR_{DTS}), available energy was partitioned into sensible
 (H) and latent heat (LE) fluxes (Fig. 5 and Fig. A2 in the appendices). The H and LE co-varied
 with latent heat predominantly exceeding sensible heat across phenophases. On days with
 precipitation (P) the H and LE appeared to be equally partitioned.

575



580

585

590

595

Figure 5. Daily meteorological conditions at the Mpika study site in the Luangwa Basin for the period May 2021 – December 2021. Shaded area for variables is the standard deviation. Shaded area May-June is the canopy Green-down phenophase, July-September is the dormant phenophase and October-December is the Green-up phenophase.

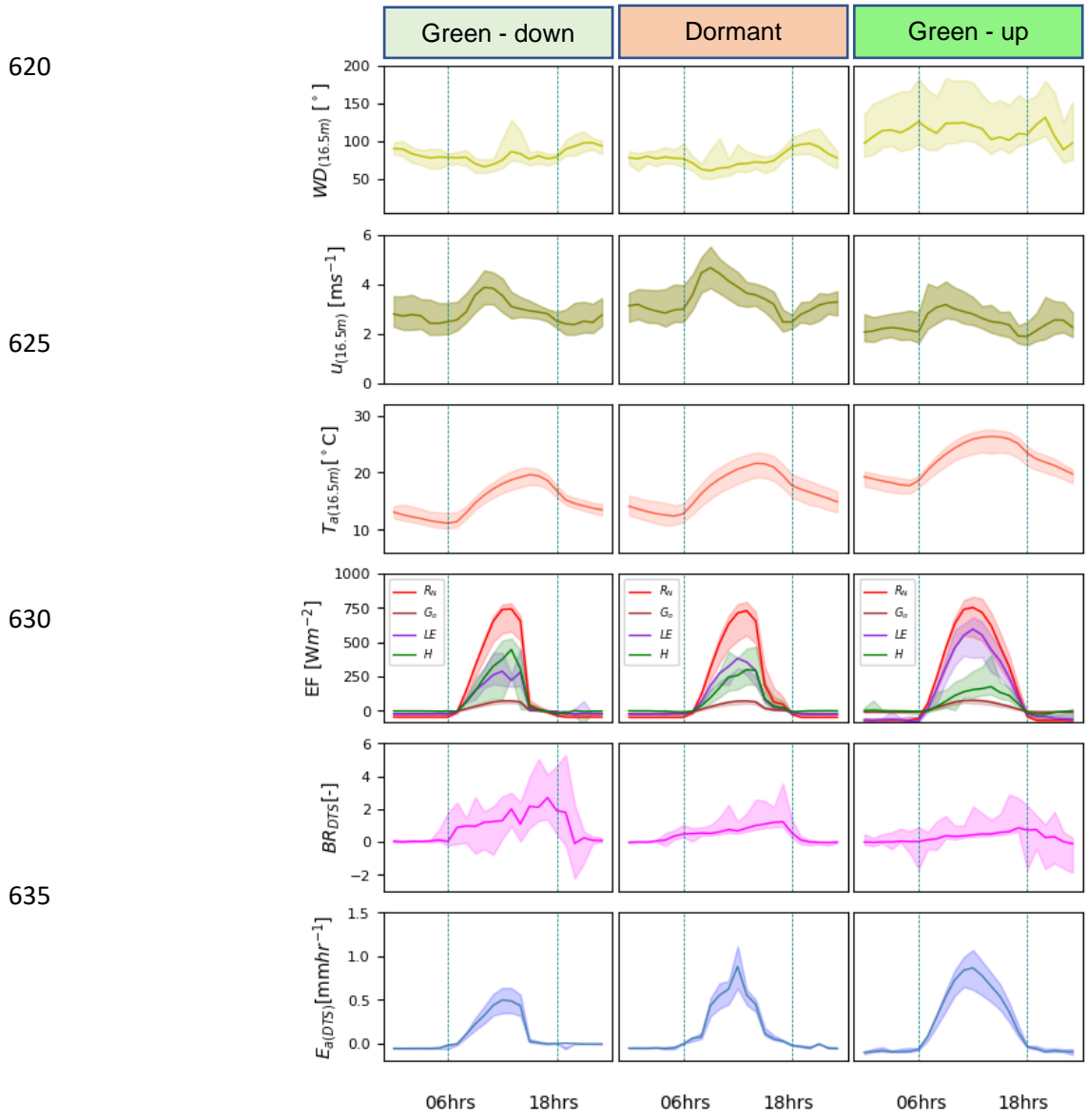
3.5 Canopy phenophase based Bowen ratio and evaporation pattern

During the green-down phenophase the Bowen ratio was highest while air temperature was lowest in a relatively lower net radiation and vapour pressure environment. During the dormant and green-up phenophases the Bowen ratio was lowest while the temperature was highest in relatively higher net radiation and lower relative humidity conditions (Figs. 5, 6 and Fig. A2 in the appendices). The green-down phenophase (i.e., May-June) showed the lowest air temperature and net radiation (Figs. 5 and 6) and exhibited the highest mean diurnal Bowen ratio (BR) (i.e., diurnal mean BR ≈ 1.3) indicative of the energy being largely expended as sensible heat compared to the dormant (i.e., diurnal mean BR ≈ 0.27) and green-up (i.e., diurnal mean BR ≈ 0.35) phenophases with raised air temperature and net radiation when the energy was mainly expended as latent heat (i.e., diurnal mean BR < 0.4) (Figs. 5 and 6). Alternating energy partitioning was detected across

605

610

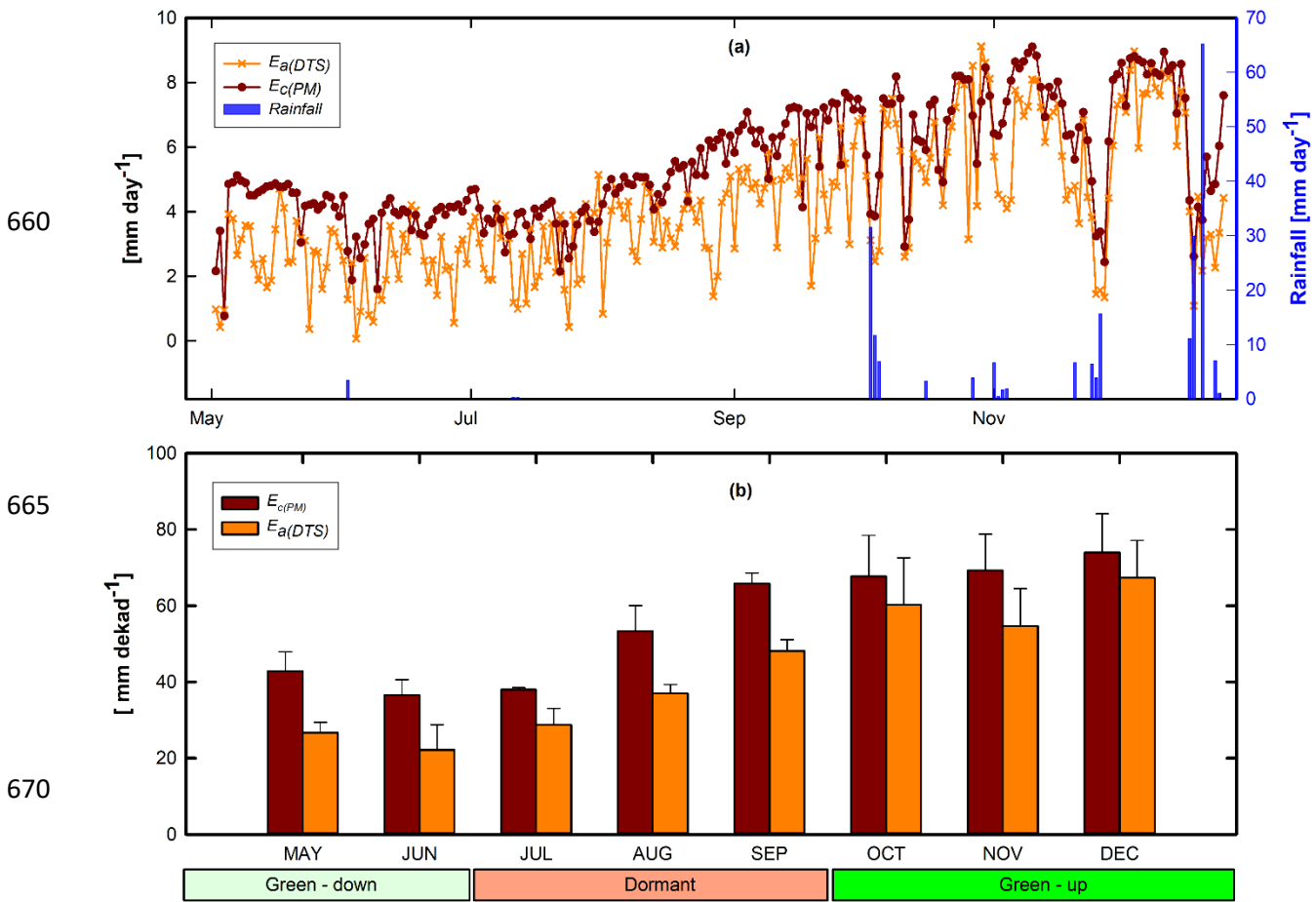
615 the phenophases as can be seen through the mean Bowen ratio, sensible and latent heat fluxes (Figs. 5 and 6). Diurnal energy partitioning interchange, across the three phenophases, occurred round 06 AM and 6PM (Fig. 6). The study site is situated in a warmer Miombo region (Chidumayo and Gumbo, 2010). The observed alternating energy partitioning (i.e., Bowen ratio) pattern is similar to what has been observed in warm ecosystems and climates (i.e., Cho *et al.*, 2012) such as the Miombo ecosystem. Consequently, diurnal evaporation pattern at the study site is dependent on daily energy partitioning, increasing with net radiation and air temperature (Figs. 5 and 6).



640 **Figure 6.** Forest canopy phenophase based hourly averages of wind direction (WD), wind speed (u), Energy flux (EF) (net radiation (R_N), ground heat flux (G_o), latent heat flux (LE) and sensible heat flux (H)), Bowen ratio (BR_{DTS}) and actual evaporation ($E_{a(DTS)}$). Shaded area is the standard deviation.

3.6 Comparison of daily potential evaporation and actual evaporation

645 $E_{a(DTS)}$ was estimated at diurnal (06 AM – 6 PM) hourly interval and then summed up into daily and dekadal estimates. Overall, daily $E_{c(PM)}$ was higher than $E_{a(DTS)}$ by an average of 17 percent (Fig. 7 a). However, under low temperature conditions (i.e., June – July) on some days the $E_{a(DTS)}$ was higher than the $E_{c(PM)}$ (Fig. 7 a). In higher air temperature and low forest canopy cover (i.e., in the dormant phenophase August and September), $E_{c(PM)}$ was higher than $E_{a(DTS)}$. The soil water limitations and changes in leaf colour (Fig. 8 and Fig. A3 in the appendices) may have resulted in significantly higher $E_{c(PM)}$ compared to $E_{a(DTS)}$. The $E_{a(DTS)}$ and $E_{c(PM)}$ showed similar behaviour across canopy phenophases with strong correlation ($r = 0.95$) at dekadal scale (Fig. 7 b and Table A4 in the appendices). For both $E_{a(DTS)}$ and $E_{c(PM)}$, significant variations (i.e., coefficients of variations and standard deviations) were observed in the green-up phenophases (i.e., October – December) (Fig. 7 b, Table A3 in the appendices).



675 **Figure 7.** (a) May – December 2021 daily (6AM - 6PM) estimates of evaporation $E_{a(DTS)}$ using the $BR-DTS$ and $E_{c(PM)}$ using the PM . (b) Comparison of dekadal evaporation estimates between $E_{a(DTS)}$ estimates and $E_{c(PM)}$ ($E_c = K_c \cdot E_o$). The $E_{a(DTS)}$ and $E_{c(PM)}$ show good agreement in both dry and rainy seasons as well as across canopy phenophases. Overall, at dekadal scale the $E_{c(PM)}$ is relatively higher than $E_{a(DTS)}$ (b). Phenophases classification: May-June is the green-down phenophase, July-September is the Dormant phenophase and October-December is the green-up phenophase.

680

685

690

695

700

705

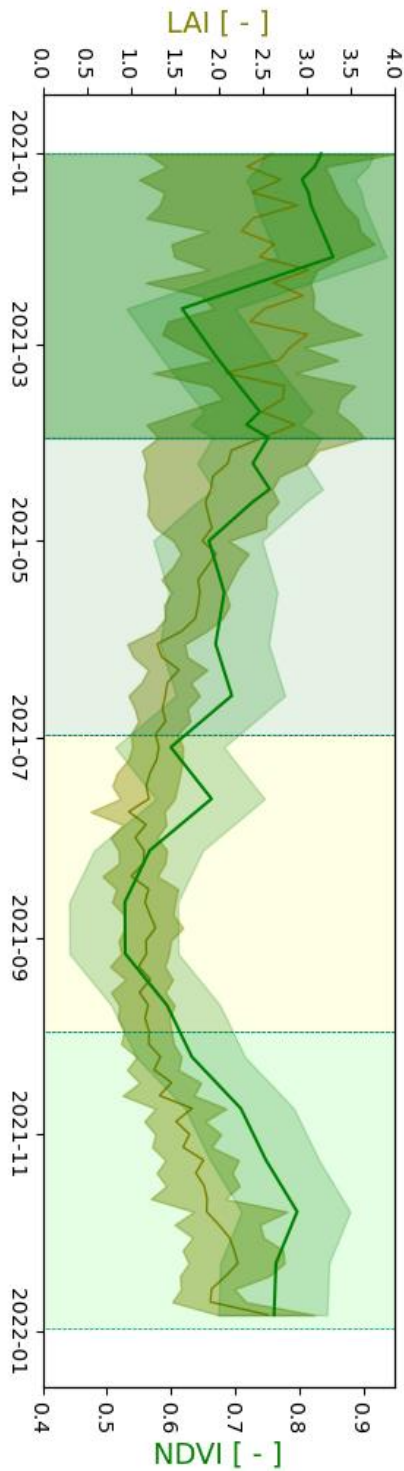


Figure 8. Selected aerial view images of the upwind direction (East direction) above the forest canopy from the flux tower across phenophases from January-December 2021. The differences in forest cover leaf colour display at the study site are clearly demonstrated across phenophases. The satellite-based *NDVI* and *LAI* appear to agree with the forest canopy cover changes.



The high coefficients of variations in the dormant and green-up phenophases could have been caused by changes in both meteorological conditions and forest canopy cover characteristics such as leaf fall, leaf flush and leaf colour (i.e., Figs. 5 and 8).

The $E_{a(DTS)}$ appeared to follow the trend of available energy (i.e., net radiation, air temperature) (i.e., Kendall's tau (τ) from 0.09 to 0.6) instead of the changes in forest canopy cover (i.e., Kendall's tau (τ) from 0.09 to 0.2) (Figs. 5 and 9). For instance, the lowest $E_{a(DTS)}$ was observed during the lowest net radiation and air temperature in June while the highest $E_{a(DTS)}$ was observed during the period with highest net radiation in the green-up phenophase. In the dormant phenophase, the $E_{a(DTS)}$ increased as NDVI reduced ($\tau = -0.22$). The upward trend in the dormant $E_{a(DTS)}$ even when forest canopy cover (i.e., NDVI) reduced may have been caused by the access to deep soil moisture and vegetative water storage (Tian *et al.*, 2018; Vinya *et al.*, 2018) by plants that had either not started the leaf fall or those that already acquired new leaves and had greened up (Fig. 8). The leaf fall and leaf colour transitions (i.e., Fig. 8 and Fig. A3 in the appendices) in some Miombo species, at any given time, across the three phenophases, is compensated by the leaf flush and greening up process in other species, which ensures that about 70% evaporative surface (i.e., forest canopy cover) (Fuller, 1999, Frost, 1996 and Fig. 8) is available at any period of the year. The forest canopy cover percentage increases as the phenophases transition from dormant to the peak phenophase (i.e., Fig. 8 and Fig. A3 in the appendices). Zimba *et al.* (2020) showed that August/September and not June, had the highest plant water stress (i.e., lowest NDII (Sriwongsitanon *et al.*, 2015)). June showed the lowest net radiation and air temperature (Fig. 5). However, $E_{a(DTS)}$ for August/September was higher than that for June. This dormant phenophase $E_{a(DTS)}$ behaviour demonstrates available energy, coupled with adapted physiological processes, as the possible main driver (s) of the Miombo forest evaporative dynamics.

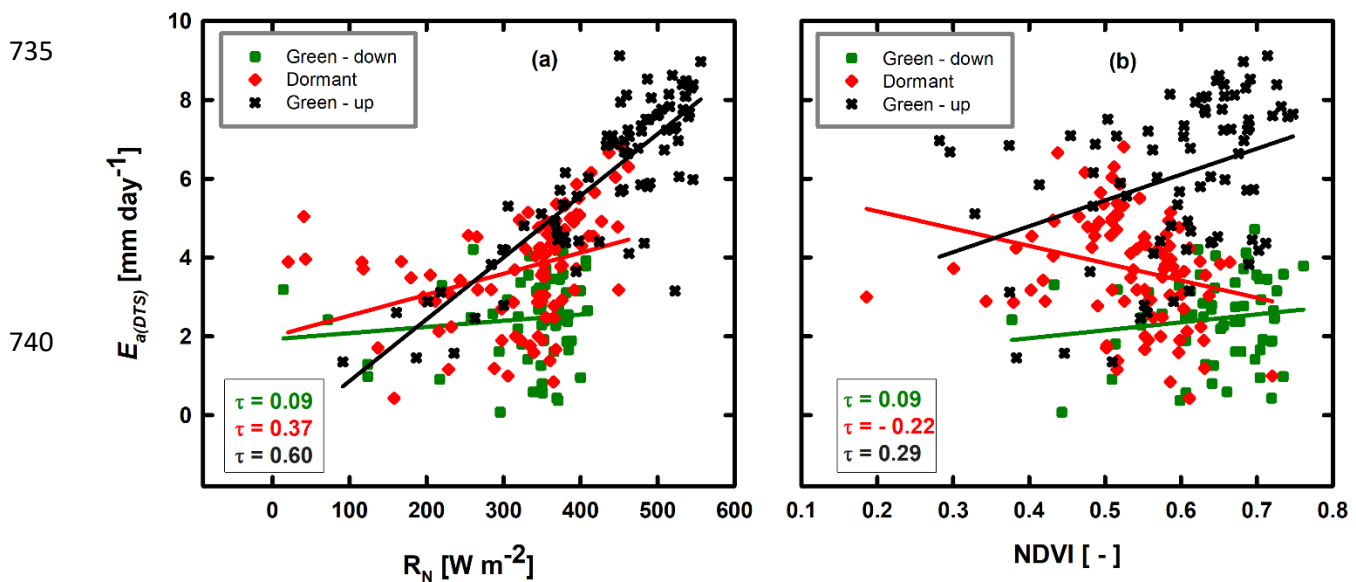


Figure 9. Kendall correlation of $E_{a(DTS)}$ with R_N and $NDVI$ in the Green-down, Dormant and Green-up phenophases of the Miombo forest at Mpika site, Zambia.

In the green-up phenophase, $E_{a(DTS)}$ increased with increase in net radiation and NDVI ($\tau = 0.60$; 0.29 respectively) (Fig. 9). The highest net radiation and air temperature were observed in

750 the green-up phenophase (Fig. 5). The NDII values (i.e., vegetation water content) started to rise in September (Zimba *et al.*, 2020). The increase in the E_a (DTS) from July was sustained through October to December (green-up phenophase) (Fig. 7), before the commencement of stable rains. The NDII trend in the green-up phenophase may have been as a result of the increased forest canopy cover (Fig. 8) with access to deep soil moisture/ground water and vegetative storage. The E_a (DTS) green-up phenophase trend could have been caused by increased vegetation water content and available energy. The marginal drop of E_a (DTS), in November, at the start of the ~~rain~~ season, could be attributed to the drop in net radiation and air temperature (Fig. 5) influenced by cloud cover and rainfall activity (Fig. 7 a). During increased rainfall activity, atmospheric water demand may have been lowered as relative humidity increased while net radiation reduced (Fig. 5). The same explanation holds for the E_a (DTS) estimates in December.

760 3.7 Comparison of satellite-based evaporation estimates to field observations

760 3.7.1 Comparison of temporal trend and magnitude

765 Among the four satellite-based evaporation estimates, only the WaPOR showed similar trend to field observations across the three phenophases (May to December) with strong correlation coefficients ($r = 0.85, 0.83$ with E_a (DTS) and E_c (PM) respectively) (Fig. 10 and Table A4 in the appendices). This was followed by SSEBop ($r = 0.51, 0.58$ with E_a (DTS) and E_c (PM) respectively), while the MOD16 showed the weakest correlation ($r = 0.01, -0.01$ with E_a (DTS) and E_c (PM) respectively). In contrast, the ~~GLEAM~~ showed a negative correlation with both E_a (DTS) and E_c (PM) observations ($r = -0.53, -0.78$ with E_a (DTS) and E_c (PM) respectively) (Fig. 10 and Table A4 in the appendices). With an exception of the WaPOR, diversion from observed E_a (DTS) and E_c (PM) begun in July at the commencement of the rise in air temperature and net radiation, increased wind speed and the beginning of the dormant phenophase (i.e., typified by leaf fall, leaf flush and leaf colour change activities (Figs. 5, 8 and 10). Surprisingly, the GLEAM appeared to strongly underestimate actual evaporation during the dormant and green-up phenophases (Fig. 10).

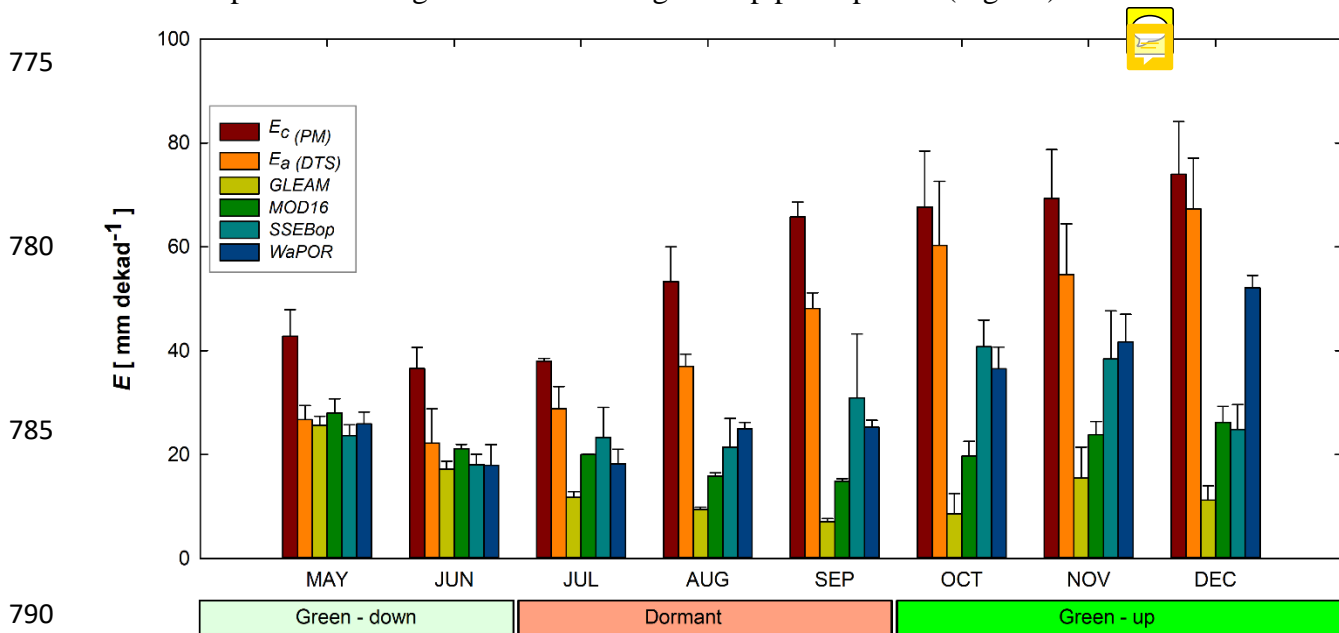


Figure 10. Bar graphs with standard deviation error bars comparing dekadal averages of E_a (DTS) and E_c (PM) with satellite-based evaporation estimates from May – December 2021. The WaPOR shows a similar trend to both E_a (DTS) and E_c (PM).


3.7.2 Phenophase-based cumulative estimates and coefficients of variations

795 Between 1st May to 20th December, 2021, observed actual evaporation $E_{a(DTS)}$ was about 24 percent lower than the estimated potential evaporation $E_{c(PM)}$ (Table 2). The largest difference (approximately 130 mm) between $E_{c(PM)}$ and $E_{a(DTS)}$ was in the water limited dormant phenophase in the dry season proper.

800 Table 2. Comparison of the 2021 monthly cumulative evaporation at Mpika Miombo forest site

Product	Phenophase mean actual evaporation estimate (mm phenophase ⁻¹)				Satellite product % lower than $E_{a(DTS)}$	Satellite product % lower than $E_{c(PM)}$
	Green-down	Dormant	Green-up	Total		
$E_{a(DTS)}$	146.62	341.75	479.47	967.83		
$E_{c(PM)}$	237.86	471.32	558.88	1268.06		
GLEAM	128.22	84.69	94.25	307.16	68.26	75.78
MOD16	147.44	152.14	182.75	482.33	50.16	61.96
SSEBop	124.99	226.72	287.05	638.76	34.00	49.63
WaPOR	131.40	204.93	338.64	674.97	30.26	46.77

805 Over the same period, cumulative average GLEAM actual evaporation was about 76 percent lower than potential evaporation and 68 percent lower than $E_{a(DTS)}$. MOD16 was about 62 percent lower than potential evaporation and 50 percent lower than actual evaporation $E_{a(DTS)}$. The SSEBop was about 50 percent lower than potential evaporation and 34 percent lower than actual evaporation $E_{a(DTS)}$. WaPOR was about 46 percent lower than potential evaporation and 30 percent lower than actual evaporation $E_{a(DTS)}$ (Table 2). The green-down phenophase showed the least differences between satellite-based evaporation estimates and field observations (Table 2). Overall, the four satellite-based estimates underestimated actual evaporation across the forest canopy phenophases (Fig. 10 and Table 2). However, in the green-down all four satellite-based estimates showed similar behaviour (i.e., trend and magnitude) with the $E_{a(DTS)}$ (Fig. 10 and Table 2).

810 The green-down phenophase showed the lowest coefficient of variation among the four satellite products (Fig. 11). The low coefficient of variation coupled with the low underestimation in the green-down phenophase showed that satellite-based estimates are closer to Miombo forest actual evaporation in conditions of high forest canopy cover and high soil moisture content in the sub-surface. The dormant and green-up phenophases showed large underestimation and large coefficients of variation among the satellite-based estimates (Table 2 and Fig. 11). The underestimation during the green-up phenophase may be caused by difficulty of modelling interception, especially in October and November at the beginning of the rain season. The significant variations in dormant phenophase actual evaporation estimates showed that satellite products have difficulty estimating Miombo forest evaporation in conditions with low forest canopy cover (with associated changes in leaf display characteristics), high available energy, and low soil moisture content in the upper layers of the soil. If canopy transpiration is not coupled with access to deep soil moisture beyond 250 cm,  is the case with the GLEAM, satellite-based estimates are likely to underestimate dormant phenophase Miombo forest actual evaporation.

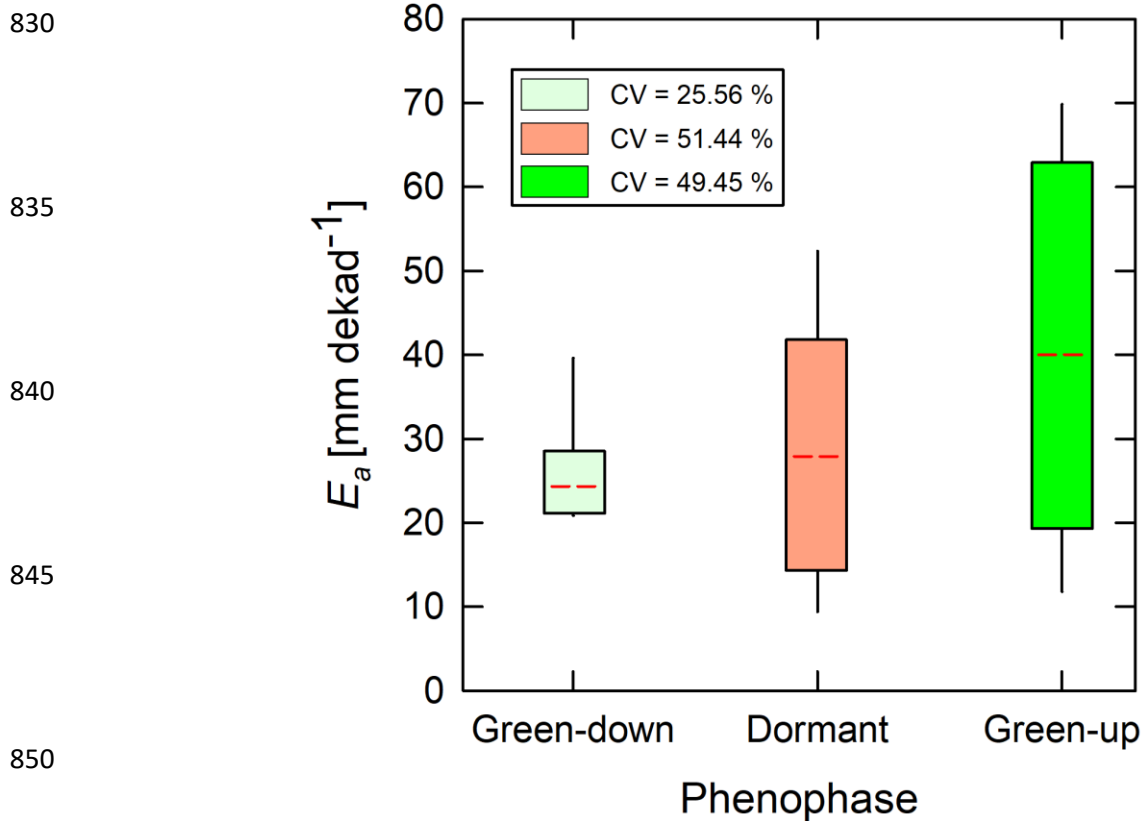


Figure 11: Box plots showing variations in satellite-based evaporation estimates at dekad scale across phenophases. Dotted red line is the mean for each phenophase. Coefficients of variation (CV) were largest during the dormant and green-up phenophases.

3.7.3 Performance statistics of satellite-based estimates with reference to BR-DTS estimates

Overall, for the eight-month period, the WaPOR showed the lowest underestimation (i.e., MBE), had the highest correlation coefficient and lowest RMSE. The WaPOR was followed by the SSEBop and then MOD16. The GLEAM showed the lowest estimates, high RMSE and largest MBE. Only the WaPOR consistently showed positive correlation (r) with field observations across the three phenophases (Fig. 12 a). The underestimations were mainly associated with the dormant and green-up phenophase (Fig. 10), as can be seen from the uncertainty RMSE and MBE values in Fig. 12 b, c. Therefore, for satellite-based estimates, it appears the dormant and green-up phenophases are the most difficult to assess. The SSEBop and WaPOR estimates appeared closer to dry season Miombo forest actual evaporation than the MOD16 and GLEAM. The behaviour, in terms of trend and magnitude, of satellite-based evaporation estimates in relation to field observations of the Miombo forest actual evaporation may be attributed to individual satellite product characteristics.

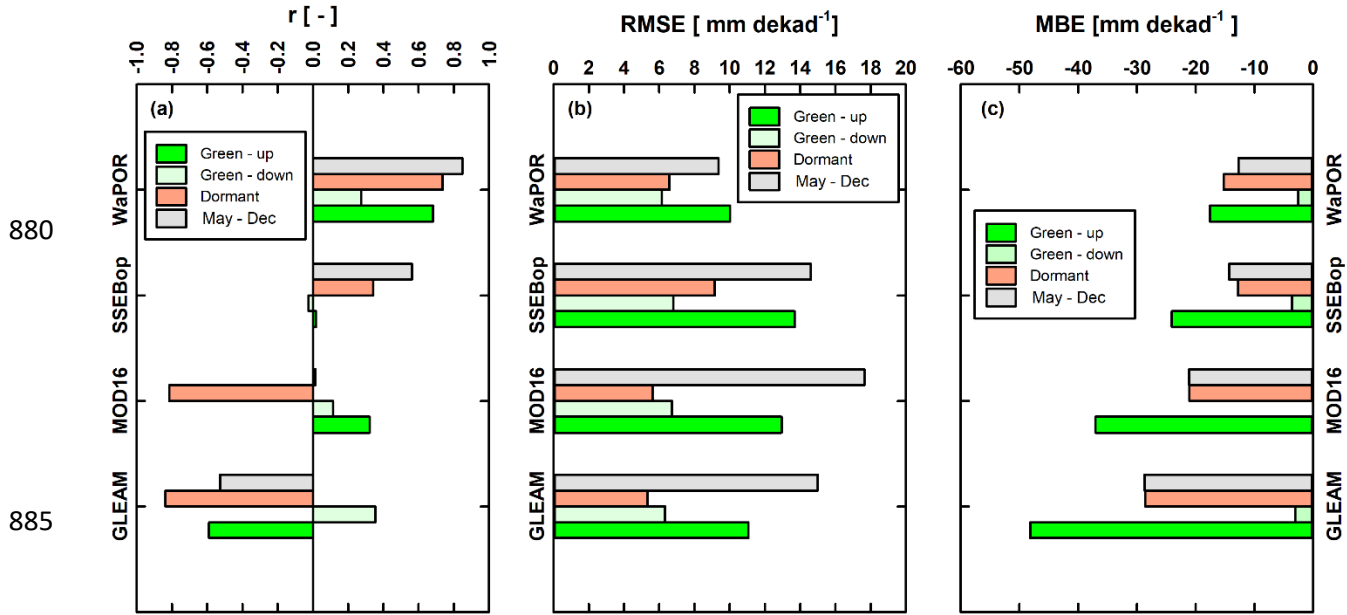


Figure 12: (a) statistics of the correlation of $E_{a(DTS)}$ with satellite-based estimates and (b, c) statistics of uncertainty in satellite-based evaporation estimates with reference to $E_{a(DTS)}$ for each phenophase and for the entire study period May-December, 2021.

4 Potential causes of the discrepancies between $E_a(DTS)$ and satellite-based estimates

4.1 Global Land Evaporation Amsterdam Model (GLEAM)

GLEAM has four modules that are used to obtain actual evaporation. The modules include the potential evaporation, rainfall interception, soil and stress modules. The potential evaporation module uses the Priestly and Taylor equation, and is driven by observed surface meteorology. The interception module is based on the Gash analytical model, and is driven by observed precipitation. The soil module is a multi-layer model driven by observed precipitation and satellite surface soil moisture. The stress module is based on semi-empirical relation to root zone soil moisture and the vegetation optical depth (VOD) (Martens *et al.*, 2017).

GLEAM's green-down phenophase behaviour was similar to both field observations and other satellite-based evaporation estimates. However, GLEAM's behaviour, in low soil moisture and low forest canopy cover dormant phenophase, was different, both in terms of trend and magnitude. This showed GLEAM's sensitivity to changes in the sub-surface moisture dynamics. GLEAM soil module only takes into account 250 cm of the sub-surface soil moisture that is linked to observed precipitation. GLEAM drainage algorithm does not take into account horizontal and upward moisture fluxes beyond 250 cm depth. This implies that GLEAM is fully based on net precipitation, thereby not taking into account the groundwater fluxes that are not related to precipitation. At the study site, and the Miombo Woodland in general, the green down and dormant phenophases occurs in the dry season. The soil moisture (i.e., at 30 cm) begins to decline in March at the end of the rain season but stays relatively unchanged throughout the dry season (Fig. 5). However, the moisture residue at 30 cm subsurface is higher during the green-down phenophase as compared to the dormant and start of the green-up phenophases (Fig. 5 and Chidumayo, 2001). Studies (e.g., Gumbo *et al.* 2018; Tian *et al.*, 2018; Vinya *et al.*, 2018; Guan *et al.*, 2014; Frost, 1996; Savory, 1963) showed that Miombo species have vegetative water storage mechanisms as

well as deep (beyond 5 m depth in some species) and extensive lateral rooting system providing accessing to ground water resources. This explains the behaviour of field observations which showed a rise in evaporation during the dormant and green-up phenophases in the dry season. The rise in GLEAM actual evaporation in October could be attributed to the interception, due to rainfall activity, and the sporadic rise in soil moisture in October (Fig. 5). This validates GLEAM's dependence on net precipitation for actual evaporation assessment. In increased solar radiation and canopy cover (i.e., leaf area index (LAI)) conditions, i.e., in October at the study site, a small amount of precipitation is likely to result in high interception, and only begins to reduce as precipitation increases. This shows that the GLEAM interception module, aided by the use of good quality rainfall product, i.e., Multi-Source Weighted-Ensemble Precipitation (MSWEP), is responsive in the Miombo forest.

The overall driving factor of GLEAM's actual evaporation estimates, with reference to the $E_{a(DTS)}$ in this study, might be the accuracy of the vegetation fraction product used in GLEAM, in this case the Global Vegetation Continuous Fields product (MOD44B). Since the evaporative flux components (i.e., interception loss, soil evaporation and transpiration as well as potential evaporation estimates) are all based on the vegetation fraction cover, the accuracy of the vegetation fraction product is a key factor in the overall accuracy (in relation to the Miombo ecosystem) of the estimated actual evaporation for each land cover. The GLEAM is based on four land cover classifications that include bare soil, low vegetation (i.e., grass), tall vegetation (i.e., trees), and open water (i.e., lakes). Misclassification of the land cover type will have a cascaded effect on several components of the model, including the interception loss estimation and the multiplicative stress factor which influences the estimation of the various evaporation components in the model.

4.2 MODerate resolution Imaging Spectroradiometer (MOD16)

The MOD16 evaporation algorithm is based on the Penman-Monteith equation (Monteith, 1965). The model computes actual evaporation as a summation of plant evaporation (canopy interception and transpiration) and soil evaporation utilising both remote sensing and meteorological inputs (Mu *et al.*, 2011). In the green-down phenophase MOD16 showed similar behaviour, in terms of trend and magnitude, with $E_{a(DTS)}$. However, in the dormant phenophase MOD16 had a different trend from $E_{a(DTS)}$ and underestimated actual evaporation. In the green-up phenophase MOD16 showed a trend similar to $E_{a(DTS)}$ but underestimated evaporation. Potential evaporation ($E_c(PM)$) and actual evaporation ($E_{a(DTS)}$) showed lowest evaporation estimates in June (Figs. 7 and 10). In contrast, the MOD16 showed September with the lowest estimates of actual evaporation (Fig. 10). This was two months delay. During the dormant phenophase (i.e., dry season proper) Miombo forest actual evaporation is through the transpiration process. At Mpika's Miombo forest site, Zimba *et al.* (2020) showed lowest LAI and NDVI values in August and September respectively. The MOD16 actual evaporation trend agreed with the vegetation indices, LAI and NDVI. However, net radiation and air temperature started to increase in July (Fig. 5). At the Mpika Miombo forest, Zimba *et al.* (2020) showed long-term average, 2009-2020, NDVI of about 0.5 in July. The July NDVI value was indicative of presence of green health vegetation. Furthermore, the normalised difference infrared index (NDII) indicated that lowest soil moisture and maximum plant water stress was reached in August/September (i.e., Sriwongsitanon *et al.*, 2015; Zimba *et al.*, 2020). Additionally, Miombo species dry season plant water interactions have been sufficiently highlighted (e.g., Gumbo *et al.* 2018; Tian *et al.* 2018; Vinya *et al.* 2018; Frost 1996, Savory, 1963). Therefore, the start in increase in air temperature and net radiation (indicative of available energy) in July is before the plants are highly water stressed, and might be the correct start in rise in actual evaporation as depicted by $E_{a(DTS)}$, SSEBop and WaPOR. Consequently, if

the MOD16 energy balance module is not well adjusted for the Miombo Woodland it may be the reason for downward dormant phenophase trend of evaporation estimates.

965 The key MOD16 component during the dormant and early green-up phenophase is the
plant transpiration module driven by land cover/LAI, net radiation, air pressure, air temperature
and relative humidity. The canopy/stomata conductance thresholds are the link between the
highlighted drivers and the assessed plant transpiration. The MOD16 energy balance module and
canopy conductance may not be appropriately configured for the Miombo ecosystem. This could
970 explain why the MOD16 trend and magnitude of actual evaporation estimates differed from field
observations. Additionally, daily MOD16 evaporation is a summation of both day and night
evaporation. $E_a (DTS)$ was estimated at hourly scale between 06AM and 6PM. Actual evaporation
($E_a (DTS)$) values for day time only (about 12 hours) were different from 24-hour averages for
MOD16.

975 4.3 Operational Simplified Surface Energy Balance (SSEBop)

The SSEBop is based on the energy balance, distinguishing between hot and cold pixels to
estimate evaporation. The SSEBop actual evaporation is calculated using an evaporation fraction
that is based on the hot/dry and cold limiting conditions. To obtain actual evaporation the
evaporation fraction is multiplied with the crop coefficient (K_c) and potential evaporation (E_o)
980 (Savoca *et al.*, 2013). The SSEBop appeared to have a similar behaviour, both trend and
magnitude, with $E_a (DTS)$ during the green-down phenophase but these differed during the dormant
and green-up phenophases in August and December.

The SSEBop is sensitive to solar radiation/temperature and thus, effectively responded to
the changes in these variables (i.e., net radiation and air temperature) as they started to rise in July.
985 The marginal drop in evaporation in August could be due to the leaf shedding processes that
exposed the dry leaf and grass covered forest floor to more interaction with radiation resulting in
increased temperature. The increased soil surface temperature was interpreted by SSEBop as non-
evaporative surface. Furthermore, the drop in the SSEBop actual evaporation in August could have
been caused by the relatively (i.e., compared to the MOD16 and the WaPOR) coarser spatial
990 resolution (i.e., 1 km), the heterogeneity in the leaf fall and leaf flush trend, and the bush burns
that normally occur during this period (Gumbo *et al.*, 2018; Frost, 1996). The SSEBop
underestimation of actual evaporation in December could be attributed to two factors; cloud cover
and the uncertainties associated with estimating land surface temperature (LST) in hot humid
conditions (Dash *et al.*, 2002). There is increased cloud cover and rainfall activity in December
995 that affects the quality of the satellite LST product. The SSEBop is based on clear sky net radiation
balance principle (Savoca *et al.*, 2013). Zimba *et al.* (2020) indicated that the quality pass for the
satellite-based MODIS LST product at the study site was below 80 percent during the rainy season
(i.e., December).

With reference to the $E_a (DTS)$ the underestimation by the SSEBop could be attributed to
1000 several factors, including the quality of the satellite LST product used and the overpass time of the
MODIS satellite over the study site. The SSEBop daily evaporation estimates includes the night
time. $E_a (DTS)$ estimates were between 6AM and 6 PM. The differences in the time intervals results
in different daily actual evaporation averages contributing to the observed discrepancy. This is
even more important when the 10AM and 1 PM overpass time for MODIS Terra and Aqua is
1005 considered. The overpass time affects the minimum and maximum LST estimation which
influences estimated SSEBop actual evaporation.

4.4 Water Productivity through Open access Remotely sensed derived data (WaPOR)

1010 The WaPOR is the only one of the four satellite-based evaporation estimates which showed
similar trend with $E_a(DTS)$ across phenophases and had very strong correlation ($r = 0.85$) (Fig. 10
and Table A4 in the appendices). ~~It significantly~~ underestimated actual evaporation in the
dormant and green-up phenophases. The WaPOR is based on satellite estimates from the modified
1015 Penman-Monteith (P-M) ETLook model which has been adapted to remote sensing inputs
(Blatchford *et al.*, 2020; FAO, 2018). The actual evaporation is estimated based on seven data
components which include precipitation, surface albedo, solar radiation, NDVI, soil moisture
stress, land cover and weather data. The WaPOR actual evaporation is a summation of interception,
soil evaporation and canopy transpiration. In the WaPOR transpiration is coupled via the root zone
1020 soil moisture content while soil evaporation is coupled via the top soil moisture content. The Net
radiation is split into soil and canopy net radiation. This implies that increase in LAI exponentially
reduces available soil net radiation and increases canopy net radiation. The LAI is derived from
the NDVI. The WaPOR estimates canopy resistance and establishes the coupled response of soil
moisture and LAI on transpiration. The land cover data is used to generate vegetation type
1025 dependent stomata conductance thresholds. In the WaPOR, the classes in the land cover data are
used to estimate soil and canopy roughness, while the NDVI is used to account for seasonal
variations during the growing season (Blatchford *et al.*, 2020). In estimating the soil and canopy
aerodynamic resistance, the WaPOR includes buoyance turbulence using the Monin-Obukhovi
similarity theory. The accuracy of the land cover product used influences the thresholds for stomata
1030 conductance and other land cover type related components of the model. The use of relatively high
spatial resolution Copernicus land cover product in the WaPOR, which has high forest
classification accuracy, contributes to its ability to capture the vegetation type, which coupled with
appropriate parameterisation of the stomata conductance and other vegetation related variables,
appeared to correctly model the trend of the actual evaporation in the Miombo forest.

Unlike GLEAM, the WaPOR is not a product of a fully net precipitation-based model. The
1035 ETLook model takes into account the vegetation type interaction with the sub-soil moisture
content. The soil moisture stress module appeared to correctly model the Miombo species
interactions with soil moisture across the three phenophases. Most importantly, WaPOR correctly
characterised actual evaporation trend in the dormant phenophase, which the other three satellite-
based estimates did not. Both $E_a(DTS)$ and WaPOR are dependent on correctly partitioning available
1040 energy into sensible and latent heat fluxes. Therefore, the WaPOR energy balance module
correctly partitioned energy fluxes in the Miombo forest across the three phenophases. The various
inputs and processes in the WaPOR, as described above, may explain why it showed the same
trend as the field observation and had lower underestimation of actual evaporation. Just like in the
GLEAM, MOD16 and SSEBop the underestimation by the WaPOR could have been partly due to
1045 the differences in the daily time intervals for the estimation of actual evaporation, as well as the
quality of the net radiation product used in the model. The WaPOR is estimated over a 24-hour
(day) period while $E_a(DTS)$ was estimated between 06AM and 6 PM.

4.5 Possible causes of the $E_a(DTS)$ overestimation

It appeared that the spatial resolution of satellite-based estimates was of influence, as the
1050 underestimation was clearly observable, with reference to each satellite product's spatial scale.
The correlation coefficient of -0.87 (Fig. 13) implies that the finer the spatial resolution the larger
the actual evaporation estimates. Therefore, the finer the spatial resolution the lower the

underestimation (Fig. 11 and Table 2). This indicates that at finer spatial resolutions, higher than the WaPOR's 250 m, the underestimation of actual evaporation is likely to be reduced. However, the SSEBop's higher estimates than the MOD16 may suggest that other factors other than the spatial resolution were of greater influence on the estimated evaporation.

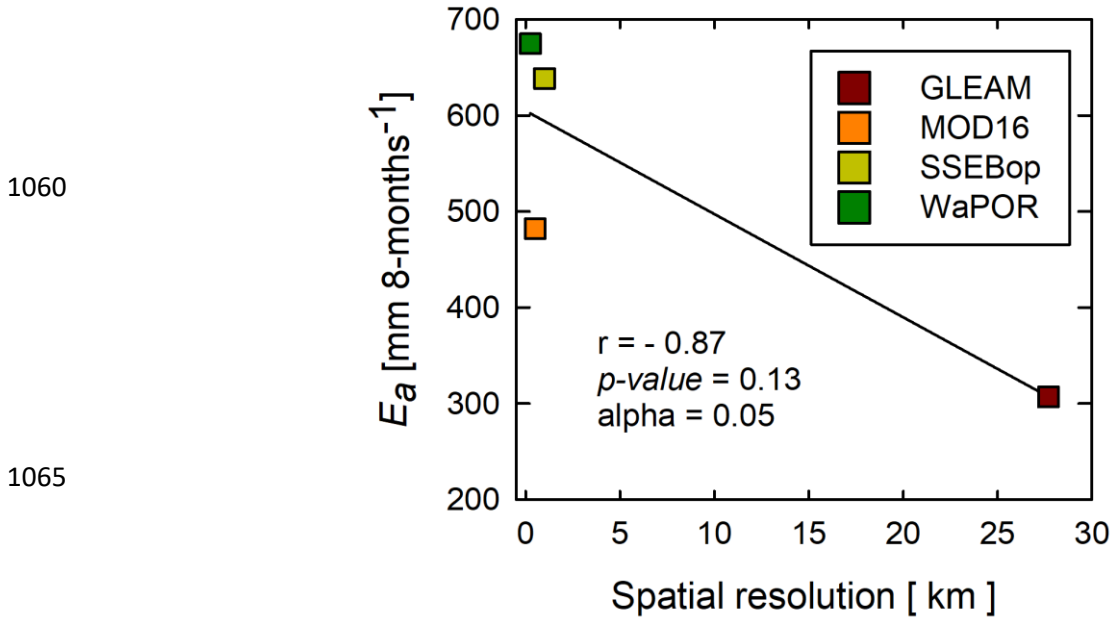


Figure 13. Point scale-based correlation of spatial resolution with estimates of actual evaporation of satellite-based evaporation estimates.

Furthermore, the ground heat flux (G_o) used in the $E_{a(DTS)}$ estimates was taken as 10 percent of the diurnal net radiation, based estimates found in other forests (i.e., Ma *et al.*, 2017; Van Der Meulen and Klaassen, 1996; McCaughey, 1982). The Miombo forest phenology is different from other ecosystems. It is possible that the G_o was underestimated, and may have contributed to the higher $E_{a(DTS)}$, as compared to the satellite-based evaporation estimates of the GLEAM, MOD16, SSEBop and WaPOR.

Another source of overestimation by the $E_{a(DTS)}$ could be the overestimation of the latent heat flux (LE) due to difficulties in flux tower instrumentation. Diurnal high temperature in the dry season (i.e., the dormant and green-up phenophases), coupled with the challenge of the constant wetting of the fibre cable for attaining wet bulb temperature, could have resulted in overestimation of the actual vapour pressure, and consequently underestimated the Bowen ratio. Underestimating the Bowen ratio could have resulted in overestimating diurnal latent heat flux, therefore, overestimating the diurnal hourly actual evaporation. This suggestion agrees with the observation by Schilperoort *et al.* (2018) which showed that, compared to the EC approach, the BR-DTS method slightly overestimated diurnal LE by a mean difference of 18.7 Wm^{-2} .

However, using the water balance approach, Zimba *et al.* (2022) showed that satellite-based estimates generally underestimated actual evaporation in the largely Miombo forest covered Luangwa Basin. Therefore, the outcome of this study's comparison of point-based field observations with satellite-based estimates, agreed with the larger picture at the Luangwa Basin scale. Consequently, the trend and magnitude of satellite-based evaporation estimates, across

1090 various Miombo strata, are likely to be the same as what this current study has observed. Nevertheless, to consolidate the observations of this study, further studies, such as this one, are needed in the different Miombo forest stratifications in Africa.

5 Conclusions and recommendations

1095 The study characterised evaporation across three forest canopy phenophases of the Miombo forest at point scale using the BR-DTS approach. Consequently, four satellite-based evaporation estimates were compared to the field observations. Major conclusions from our study are that:

Despite the dry season challenge with consistently wetting the fibre optic cable, the BR-DTS approach can be used to successfully estimate actual evaporation across different canopy phenophases of the Miombo forest.

1100 The actual evaporation trends appeared to be rather more influenced by the available energy for evaporation than the changes in the characteristic forest canopy cover dynamics during the three phenophases. This is because across the three phenophases analysed, actual evaporation had higher correlation with the net radiation trend than the changes in forest cover (proxied by the NDVI).

1105 Coupling the canopy transpiration with the root zone storage, taking into account the vertical upward (beyond 2.5 m) and horizontal soil moisture flux is likely to improve satellite-based dry season actual evaporation estimates in the Miombo forest. This is because during the dry season, i.e., dormant phenophase, field actual evaporation estimates were higher than satellite-based evaporation estimates. The Miombo forest dry season actual evaporation behaviour, i.e., trend and magnitude, is linked to the developed dry season water stress buffering mechanism (i.e., leaf fall, leaf flush and access to ground water or vegetative water storage).

1110 Phenology plays a role in satellite-based actual evaporation estimates of the Miombo forest. This is evidenced by the phenophase dependent variations (i.e., coefficients of variation) in satellite-based evaporation estimates. Some phenophases (i.e., dormant and green-up) had higher coefficients of variation compared to the green-down phenophase.

1115 Compared to field observations ($E_{a(DTS)}$) all satellite-based evaporation estimates underestimated actual evaporation. However, this result could have been influenced by the $E_{a(DTS)}$ assessment time intervals, errors in flux tower instrumentation, spatial resolution of satellite-based estimates, and the ground heat flux used in the $E_{a(DTS)}$ estimates.

1120 Consequently, of the four satellite products considered in this study, only the WaPOR showed the same trend as field observations of the actual evaporation of the Miombo forest across the three phenophases. The WaPOR highly correlated with the field observations. The WaPOR also showed the least underestimation. For the wet Miombo forest, as was represented by this study site, and limited to the four satellite-based estimates assessed, the WaPOR represents a better choice for use across the assessed Miombo phenophases. With inference based on the WaPOR, it appears that satellite-based estimates made at a scale that takes into account the local variations in the input variables might give better results.

1125 There is need for observations, such as found in the current study, to be conducted in the drier Miombo forest and to compare the results. This is because this study was conducted in the wet Miombo forest; therefore, it is possible that the phenological response to changes in hydrological regimes in the drier Miombo forest will differ from the observations at the Mpika site.

Author contribution

1135 Conceptualization, H.Z.; formal analysis, H.Z., B.S; resources, H.S.; supervision, M.C.-G. and B.K.; writing—original draft, H.Z.; writing—review and editing, M.C.-G., B.K., H.S., B.S., I.N., and N.V. All authors have read and agree to the published version of the manuscript.

Funding

1140 This study was conducted with the financial support of the Dutch Research Council (NWO) under the project number W 07.303.102.

Acknowledgements

1145 This study is part of the ZAMSECUR Project, which focuses on observing and understanding the remote water resources for enhancing water, food, and energy security in Lower Zambezi Basin We wish to thank the Water Resources Management Authority (WARMA) in Zambia for the field discharge data used in this study.

1150 The authors wish to thank Nsasala Conservancy in Mpika, Zambia for hosting the research throughout the study period. We wish to thank the Manager for the valuable contribution in local plant species identification and for maintaining the study site and equipment. This study would not have been possible without the input of the conservancy.

Conflict of interest:

1155 At least one of the (co-)authors is a member of the editorial board of Hydrology and Earth System Sciences.

1160

1165

1170

1175

1180 **Appendices**

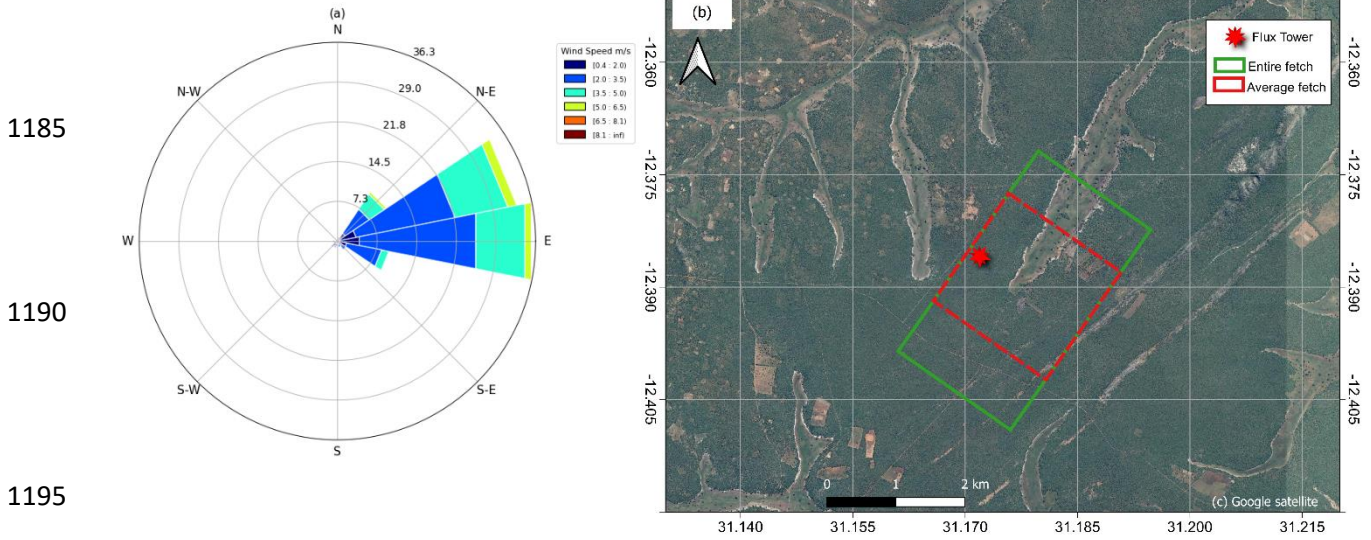


Figure A1. Analysis of the wind direction and wind speed using the wind rose (a) and the extent of the fetch for the DTS observations (b) based on the wind rose results.

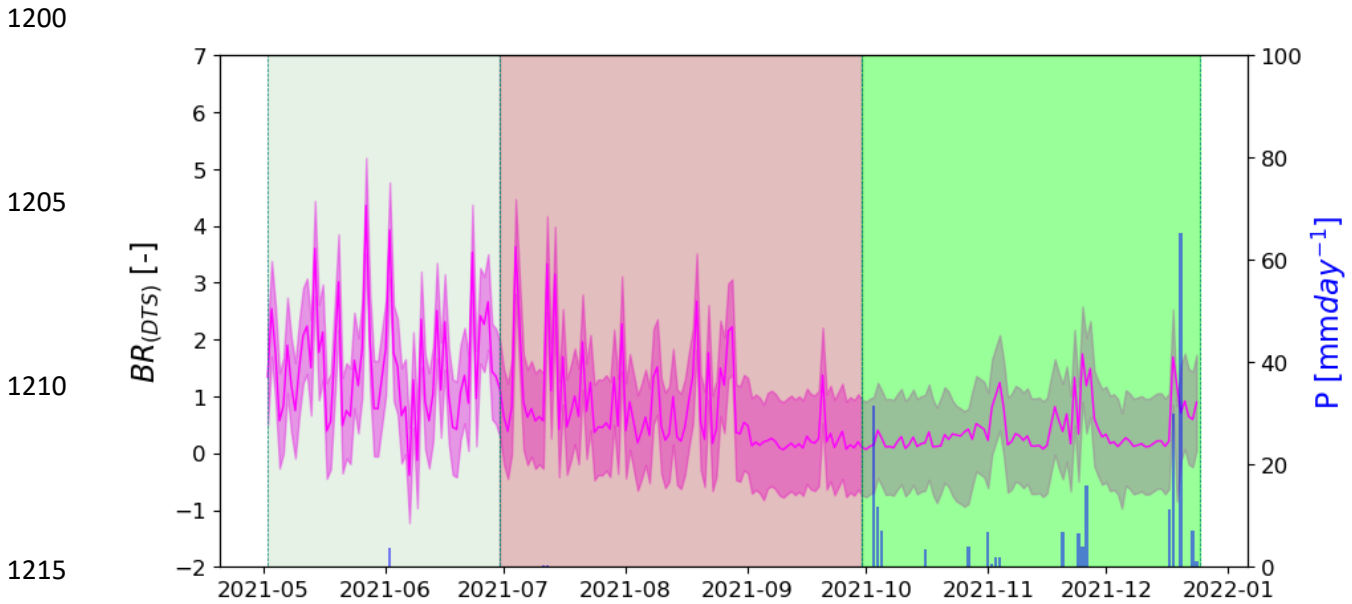


Figure A2. Estimated daily diurnal (6AM – 6PM) Bowen ratio for May to December, 2021 at the Mpika Miombo forest study site. The shaded area for Bowen ratio is the standard deviation. The shaded area for dates is the phenophase (**Senescence/Green-down:** May-June; **Dormant:** July – September; **Green-up:** October – December)

1225

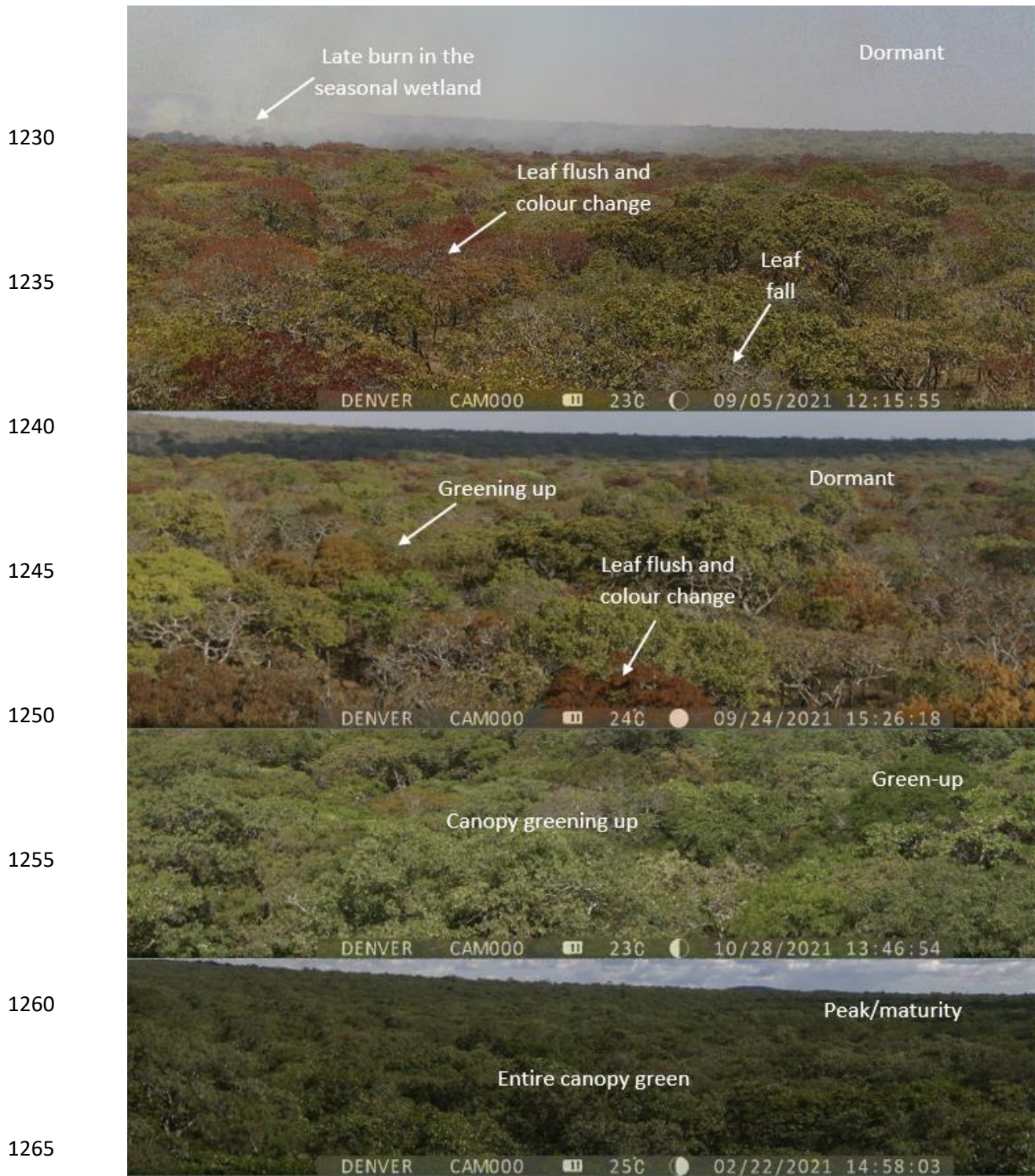


Figure A3. Photographs of the top of the forest canopy at Mpika site showing changes in canopy leaf cover in the dormant and green-up phenophases.

1270

Table A1. Sensing capabilities of the Silixa XT-DTS used in the study

Range	Channels	Resolution			Measurement time	Fiber type	Referencing
		Sampling	Temperature	Spatial			
0 – 10 km	4	25 cm	0.01°C	60 cm	≥ 5 sec	50/125µm multimode	X2 PT-100 probes

1275 **Table A2.** Selected ATMOS 41 sensor specifications

Attribute	Air temperature (°C)	Actual vapour pressure (kPa)	Relative humidity (%)	Wind speed (m/s)	Barometric pressure (kPa)
Range	-50 to 60	0 - 47	0–100% RH (0.00–1.00)	0–30 m/s	50 - 110
Resolution	0.1	0.01	0.1% RH	0.01 m/s	0.01
Accuracy	± 0.6	± 0.2 typical below 40°C (varies with temperature and humidity)	Varies with temperature and humidity, ±3% RH typical	The greater of 0.3 m/s or 3% of measurement	± 0.1 kPa from -10 to 50 °C ± 0.5 kPa from -40 to 60 °C

Table A3. Descriptive statistics of evaporation products at phenophase scale

Phenophase	Product	No. of obs	Minimum	Maximum	Sum	Mean	SD	CV
Green - down	$E_{a(DTS)}$	6	14.01	30.17	146.62	24.44	6.06	22.62
	$E_{c(PM)}$	6	30.86	47.20	237.86	39.64	6.11	14.07
	GLEAM	6	15.06	27.98	128.22	21.37	4.99	21.30
	MOD16	6	20.16	31.60	147.44	24.57	4.37	16.22
	SSEBop	6	15.92	25.34	124.99	20.83	3.77	16.53
	WaPOR	6	14.70	28.91	131.40	21.90	5.61	23.40
Dormant	$E_{a(DTS)}$	9	22.86	51.95	341.75	37.97	9.10	22.60
	$E_{c(PM)}$	9	37.34	69.46	471.32	52.37	12.84	23.12
	GLEAM	9	6.55	13.30	84.69	9.41	2.16	21.67
	MOD16	9	14.22	20.15	152.14	16.90	2.40	13.39
	SSEBop	9	15.66	46.13	226.72	25.19	9.99	37.40
	WaPOR	9	15.20	27.15	204.93	22.77	4.00	16.57
Green - up	$E_{a(DTS)}$	8	40.91	77.42	479.47	59.93	12.67	19.78
	$E_{c(PM)}$	8	56.39	84.11	558.88	69.86	11.16	14.94
	GLEAM	8	5.40	21.95	94.25	11.78	5.88	46.67
	MOD16	8	16.66	29.28	182.75	22.84	4.11	16.85
	SSEBop	8	20.09	47.33	287.05	35.88	10.11	26.36
	WaPOR	8	33.06	54.52	338.64	42.33	7.97	17.60

Table A4. Pearson r correlation coefficient of the comparison of evaporation products

Phenophase	Product	$E_{a(DTS)}$	$E_{c(PM)}$	GLEAM	MOD16	SSEBop	WaPOR
Green - down	$E_{a(DTS)}$	1.00					
	$E_{c(PM)}$	0.77	1.00				
	GLEAM	0.35	0.56	1.00			
	MOD16	0.11	0.14	0.78	1.00		
	SSEBop	-0.02	0.12	0.69	0.75	1.00	
	WaPOR	0.27	0.66	0.67	0.63	0.48	1.00
Dormant	$E_{a(DTS)}$	1.00					
	$E_{c(PM)}$	0.91	1.00				
	GLEAM	-0.84	-0.91	1.00			
	MOD16	-0.82	-0.86	0.87	1.00		
	SSEBop	0.34	0.30	-0.29	-0.31	1.00	
	WaPOR	0.74	0.81	-0.61	-0.82	0.29	1.00
Green - up	$E_{a(DTS)}$	1.00					
	$E_{c(PM)}$	0.93	1.00				
	GLEAM	-0.59	-0.37	1.00			
	MOD16	0.32	0.36	0.11	1.00		
	SSEBop	0.02	0.12	-0.07	-0.76	1.00	
	WaPOR	0.68	0.72	-0.09	0.55	-0.31	1.00
May - December	$E_{a(DTS)}$	1					
	$E_{c(PM)}$	0.95	1.00				
	GLEAM	-0.53	-0.48	1.00			
	MOD16	0.01	-0.05	0.62	1.00		
	SSEBop	0.56	0.56	-0.23	-0.14	1.00	
	WaPOR	0.85	0.83	-0.16	0.35	0.48	1.00

Values in bold are different from 0 with a significance level $\alpha=0.05$

Reference

- 1285 Allen, R. G., Pereira, L. S., Raes, D., & Smith, M.: *FAO Irrigation and Drainage Paper No. 56 - Crop Evapotranspiration*. 56, 1998.
- Angus, D. E., & Watts, P. J.: Evapotranspiration - How good is the Bowen ratio method? *Agricultural Water Management*, 8(1–3), 133–150. doi: 10.1016/0378-3774(84)90050-7, 1984.
- 1290 Barr, A. G., King, K. M., Gillespie, T. J., Den Hartog, G. & Neumann, H. H.: A comparison of bowen ratio and eddy correlation sensible and latent heat flux measurements above deciduous forest. *Boundary-Layer Meteorol.* **71**, 21–41, 1994.
- 1295 Blatchford, M. L., Mannaerts, C. M., Njuki, S. M., Nouri, H., Zeng, Y., Pelgrum, H., Wonink, S., & Karimi, P.: Evaluation of WaPOR V2 evapotranspiration products across Africa. *Hydrological Processes*, 34(15), 3200–3221. doi: 10.1002/hyp.13791, 2020.

- Bowen, I. S.: The ratio of heat losses by conduction and by evaporation from any water surface. *Physical Review*, 27(6), 779–787. doi: 10.1103/PhysRev.27.779, 1926.
- 1300 Buttar, N. A., Yongguang, H., Shabbir, A., Lakhari, I. A., Ullah, I., Ali, A., Aleem, M., & Yasin, M. A. (2018). Estimation of evapotranspiration using Bowen ratio method. *IFAC-PapersOnLine*, 51(17), 807–810. doi: 10.1016/j.ifacol.2018.08.096, 2018.
- Chidumayo, E. N.: Climate and Phenology of Savanna Vegetation in Southern Africa. *Journal of Vegetation Science*, 12(3), 347. doi: 10.2307/3236848, 2001.
- 1305 Chidumayo, E. N., & Gumbo, D. J.: The dry forests and woodlands of Africa: Managing for products and services. In *The Dry Forests and Woodlands of Africa: Managing for Products and Services* (Issue September). doi: 10.4324/9781849776547, 2010.
- Cho, J., Oki, T., Yeh, P. J. F., Kim, W., Kanae, S., & Otsuki, K.: On the relationship between the Bowen ratio and the near-surface air temperature. *Theoretical and Applied Climatology*, 108(1–2), 135–145. doi: 10.1007/s00704-011-0520-y, 2012.
- 1310 Coenders-Gerrits, M., Schilperoort, B., & Jiménez-Rodríguez, C.: Evaporative Processes on Vegetation: An Inside Look. In J. T. Van Stan II, E. Gutmann, & J. Friesen (Eds.), *Precipitation Partitioning by Vegetation: A Global Synthesis* (pp. 35–48). Cham: Springer International Publishing. doi: 10.1007/978-3-030-29702-2_3, 2020.
- 1315 Dash, P., Göttsche, F. M., Olesen, F. S., & Fischer, H.: Land surface temperature and emissivity estimation from passive sensor data: Theory and practice-current trends. *International Journal of Remote Sensing*, 23(13), 2563–2594. doi: 10.1080/01431160110115041, 2002.
- 1320 Euser, T., Luxemburg, W. M. J., Everson, C. S., Mengistu, M. G., Clulow, A. D., & Bastiaanssen, W. G. M.: A new method to measure Bowen ratios using high-resolution vertical dry and wet bulb temperature profiles. *Hydrology and Earth System Sciences*, 18(6), 2021–2032. doi: 10.5194/hess-18-2021-2014, 2014.
- FAO.: WaPOR Database Methodology: Level 1 Data. In *Remote Sensing for Water Productivity Technical Report: Methodology Series*. (Issue September). Retrieved from http://www.fao.org/fileadmin/user_upload/faoweb/RS-WP/pdf_files/Web_WaPOR-beta_Methodology_document_Level1.pdf, 2018.
- 1325 Foken, T., Aubinet, M., & Leuning, R.: Eddy Covariance. *Eddy Covariance*. doi: 10.1007/978-94-007-2351-1, 2012.
- Frost, P.: The Ecology of Miombo Woodlands. In *The Miombo in Transition: Woodlands and Welfare in Africa*. Retrieved from <http://books.google.com/books?hl=nl&lr=&id=rpildJJVdU4C&pgis=1>, 1996.
- 1330 Gray, J., Sulla-Menashe, D., & Friedl, M. A.: MODIS Land Cover Dynamics (MCD12Q2) Product. *User Guide Collection 6*, 6, 8. Retrieved from https://modis-land.gsfc.nasa.gov/pdf/MCD12Q2_Collection6_UserGuide.pdf, 2019.
- 1335 Guan, K., Eric F. Wood, D. Medvigy, John. Kimball, Ming. Pan, K.K. Caylor, J. Sheffield, Xiangtao. Xu, and O.M. Jones.: “Phenology of African Savannas and Woodlands” 119: 1652–69. <https://doi.org/10.1002/2013JG002572>, 2014.

- Gumbo, D. J., Dumas-Johansen, M., Muir, G., Boerstler, F., & Xia, Z.: Sustainable management of Miombo woodlands-Food security, nutrition and wood energy. In Food security, nutrition and wood energy. (Issue March). Retrieved from www.fao.org/publications, 2018.
- 1340 Hachigonta, S., & Reason, C. J. C.: Interannual variability in dry and wet spell characteristics over Zambia. *Handbook of Environmental Chemistry, Volume 5: Water Pollution*, 32(1), 49–62. doi: 10.3354/cr032049, 2006.
- Helsel, D. R., Hirsch, R. M., Ryberg, K. R., Archfield, S. A., & Gilroy, E. J.: Statistical Methods in Water Resources Techniques and Methods 4 – A3. *USGS Techniques and Methods*, 2020.
- 1345 Hirschi M, Michel D, Lehner I, Seneviratne SI. A site-level comparison of lysimeter and eddy covariance flux measurements of evapotranspiration. *Hydrol Earth Syst Sci* 21(3):1809–1825. <https://doi.org/10.5194/hess-21-1809-2017>, 2017.
- 1350 Hunink, J.E. , Terink, W, Contreras, S, D. P.: *Scoping Assessment of Erosion Levels for the Mahale region, Lake Tanganyika, Tanzania* (Vol. 31, Issue August). Retrieved from www.futurewater.nl, 2015.
- Ma, X., Feng, Q., Su, Y., Yu, T., & Jin, H.: Forest Evapotranspiration and Energy Flux Partitioning Based on Eddy Covariance Methods in an Arid Desert Region of Northwest China. *Advances in Meteorology*, 2017. doi: 10.1155/2017/1619047, 2017.
- 1355 Martens, B., Miralles, D. G., Lievens, H., Van Der Schalie, R., De Jeu, R. A. M., Fernández-Prieto, D., Beck, H. E., Dorigo, W. A., & Verhoest, N. E. C. (2017). GLEAM v3: Satellite-based land evaporation and root-zone soil moisture. *Geoscientific Model Development*, 10(5), 1903–1925. doi: 10.5194/gmd-10-1903-2017
- 1360 McCaughey, H. J.: Spatial Variability of Net Radiation and Soil Heat Flux Density on Two Logged Sites at Montmorency, Quebec. *Journal of Applied Meteorology*, 21, 777–787. Retrieved from <https://www.ptonline.com/articles/how-to-get-better-mfi-results>, 1982.
- Meter Group AG.: Atmos 41. In Manual (Issues 207–2022). München. Retrieved from http://library.metergroup.com/Manuals/20635_ATMOS41_Manual_Web.pdf, 2020.
- 1365 Miralles, D. G., R. A.M. De Jeu, J. H. Gash, T. R.H. Holmes, and A. J. Dolman.: “Magnitude and Variability of Land Evaporation and Its Components at the Global Scale.” *Hydrology and Earth System Sciences* 15 (3): 967–81. <https://doi.org/10.5194/hess-15-967-2011>, 2011.
- Monteith, J. L.: Evaporation and environment. *Symposia of the Society for Experimental Biology*, 19, 205, 1965.
- 1370 Mu, Q., Zhao, M., & Running, S. W.: Improvements to a MODIS global terrestrial evapotranspiration algorithm. *Remote Sensing of Environment*, 115(8), 1781–1800. doi: 10.1016/j.rse.2011.02.019, 2011.
- 1375 Olson, D. M., Dinerstein, E., Wikramanayake, E. D., Burgess, N. D., Powell, G. V. N., Underwood, E. C., D’Amico, J. A., Itoua, I., Strand, H. E., Morrison, J. C., Loucks, C. J., Allnutt, T. F., Ricketts, T. H., Kura, Y., Lamoreux, J. F., Wettengel, W. W., Hedao, P., & Kassem, K. R.; Terrestrial ecoregions of the world: A new map of life on Earth. *BioScience*,

- 51(11), 933–938. doi: 10.1641/0006-3568(2001)051[0933:TEOTWA]2.0.CO;2, 2001.
- Ramoelo, A., Dzikiti, S., Van Deventer, H., Maherry, A., Cho, M. A., & Gush, M.: Potential to monitor plant stress using remote sensing tools. *Journal of Arid Environments*, 113, 134–144. doi: 10.1016/j.jaridenv.2014.09.003, 2015.
- 1380 Savoca, M. E., Senay, G. B., Maupin, M. A., Kenny, J. F., & Perry, C. A.: Actual Evapotranspiration Modeling Using the Operational Simplified Surface Energy Balance (SSEBop) Approach. *U.S Geological Survey Scientific Investigations Report 2013–5126*, January, 16 p. Retrieved from <http://pubs.usgs.gov/sir/2013/5126>, 2013.
- Savory B. M.: “Rooting Habits of Important Miombo Species.” Ndola, 1963.
- 1385 Schilperoort, B., Coenders-Gerrits, M., Jiménez Rodríguez, C., van der Tol, C., van de Wiel, B., & Savenije, H.: Decoupling of a Douglas fir canopy: a look into the subcanopy with continuous vertical temperature profiles. *Biogeosciences*, 17(24), 6423–6439. doi: 10.5194/bg-17-6423-2020, 2020.
- 1390 Schilperoort, B., Coenders-gerrits, M., Luxemburg, W., Rodríguez, C. J., Vaca, C. C., Savenije, H., Rica, T. D. C., Forestal, E. D. I., & Rica, C.: *Technical note : Using distributed temperature sensing for Bowen ratio evaporation measurements*. 819–830, 2018.
- Silixa Ltd.: *Silixa XT-DTS Hardware Manual Version 1.3*. Retrieved from www.silixa.com, 2016.
- 1395 Spittlehouse, D. L., & Black, T. A.: Evaluation of the bowen ratio/energy balance method for determining forest evapotranspiration. *Atmosphere - Ocean*, 18(2), 98–116. doi: 10.1080/07055900.1980.9649081, 1980.
- Sriwongsitanon, N., Gao, H., Savenije, H. H. G., Maekan, E., Saengsawang, S., & Thianpopirug, S.: The Normalized Difference Infrared Index (NDII) as a proxy for soil moisture storage in hydrological modelling. *Hydrology and Earth System Sciences Discussions*, 12(8), 8419–8457. doi: 10.5194/hessd-12-8419-2015, 2015.
- 1400 Sutanto, S. J., Wenninger, J., & Uhlenbrook, S.: Partitioning of evaporation into transpiration, soil evaporation and interception: a combination of hydrometric measurements and stable isotope analyses. *Hydrology and Earth System Sciences Discussions*, 9(3), 3657–3690. doi: 10.5194/hessd-9-3657-2012, 2012.
- 1405 Teuling, A. J.: A Forest Evapotranspiration Paradox Investigated Using Lysimeter Data. *Vadose Zone Journal*, 17(1), 170031. doi: 10.2136/vzj2017.01.0031, 2018.
- Tian, F., Wigneron, J. P., Ciais, P., Chave, J., Ogée, J., Peñuelas, J., Ræbild, A., Domec, J. C., Tong, X., Brandt, M., Mialon, A., Rodriguez-Fernandez, N., Tagesson, T., Al-Yaari, A., Kerr, Y., Chen, C., Myneni, R. B., Zhang, W., Ardö, J., & Fensholt, R.: Coupling of ecosystem-scale plant water storage and leaf phenology observed by satellite. *Nature Ecology and Evolution*, 2(9), 1428–1435. doi: 10.1038/s41559-018-0630-3, 2018.
- 1410 Tombe, B. des, Schilperoort, B. and Bakker, M.: ‘Estimation of temperature and associated uncertainty from fiber-optic raman-spectrum distributed temperature sensing’, *Sensors (Switzerland)*, 20(8). doi: 10.3390/s20082235, 2020.
- 1415

- van de Giesen, N., Steele-Dunne, S. C., Jansen, J., Hoes, O., Hausner, M. B., Tyler, S., & Selker, J.: Double-ended calibration of fiber-optic raman spectra distributed temperature sensing data. *Sensors (Switzerland)*, 12(5), 5471–5485. doi: 10.3390/s120505471, 2012.
- 1420 Van Der Ent, R. J., Wang-Erlandsson, L., Keys, P. W., & Savenije, H. H. G.: Contrasting roles of interception and transpiration in the hydrological cycle – Part 2: Moisture recycling. *Earth System Dynamics*, 5(2), 471–489. doi: 10.5194/esd-5-471-2014, 2014.
- Van Der Meulen, M. W. J., & Klaassen, W.: Soil heat flux measurements in an open forest. *Physics and Chemistry of the Earth*, 21(3 SPEC. ISS.), 101–105. doi: 10.1016/S0079-1946(97)85568-1, 1996.
- 1425 Vinya, R., Malhi, Y., Brown, N. D., Fisher, J. B., Brodrigg, T., & Aragão, L. E. O. C.: *Seasonal changes in plant – water relations in fl uence patterns of leaf display in Miombo woodlands : evidence of water conservative strategies. Fuller 1999*, 104–112. doi: 10.1093/treephys/tpy062, 2018.
- 1430 Weerasinghe, I, Bastiaanssen, W., Mul, M., Jia, L., and Griensven, A.: “Can We Trust Remote Sensing Evapotranspiration Products over Africa.” *Hydrology and Earth System Sciences* 24 (3): 1565–86. <https://doi.org/10.5194/hess-24-1565-2020>, 2020.
- White, F.: *The vegetation of Africa*. Paris: UNESCO, 1983.
- 1435 Xing, Zisheng, Lien Chow, Fan-Rui Meng, Herb W. Rees, Lionel Steve, and J. M.: Validating Evapotranspiration Equations Using Bowen Ratio in New Brunswick, Maritime, Canada. *Sensors*, 1, 412-428. Retrieved from <https://doi.org/10.3390/s8010412>, 2008.
- 1440 Zimba, H, Coenders-Gerrits, M., Banda, K., Hulsman, P., van de Giesen, N., Nyambe, I., & Savenije, H.: On the importance of phenology in the Miombo ecosystem: Evaluation of open-source satellite evaporation models. *Hydrol. Earth Syst. Sci. Discuss.*, 2022(April), 1–42. Retrieved from <https://hess.copernicus.org/preprints/hess-2022-114/%0Ahttps://hess.copernicus.org/preprints/hess-2022-114/hess-2022-114.pdf>, 2022.
- 1445 Zimba, Henry, Coenders-Gerrits, M., Kawawa, B., Savenije, H., Nyambe, I., & Winsemius, H.: Variations in canopy cover and its relationship with canopy water and temperature in the miombo woodland based on satellite data. *Hydrology*, 7(3). doi: 10.3390/HYDROLOGY7030058, 2020.

1450

